NASA CONTRACTOR REPORT

A COUPLED COMPUTER CODE FOR THE TRANSIENT THERMAL RESPONSE AND ABLATION OF NON-CHARRING HEAT SHIELDS AND NOSE TIPS

by Carl B. Moyer, Larry W. Anderson, and Thomas J. Dahm

Prepared by
AEROTHERM CORPORATION
Mountain View, Calif.
for Langley Research Center

NATIONAL AERONAUTICS AND SPACE ADMINISTRATION • WASHINGTON, D. C. • OCTOBER 1970

NASA CR-1630

A COUPLED COMPUTER CODE FOR THE TRANSIENT THERMAL RESPONSE AND ABLATION OF NON-CHARRING HEAT SHIELDS AND NOSE TIPS

By Carl B. Moyer, Larry W. Anderson,
and Thomas J. Dahm

Issued by Originator as Report No. 69-60

Prepared under Contract No. NAS 1-8501 by
AEROTHERM CORPORATION
Mountain View, Calif.

for Langley Research Center

NATIONAL AERONAUTICS AND SPACE ADMINISTRATION

For sale by the Clearinghouse for Federal Scientific and Technical Information
Springfield, Virginia 22151 – CFSTI price $3.00

ABSTRACT

The report presents the analysis background and numerical details of a computer code for the transient thermal response and ablation of non-charring heat shields and nose-tips. The controlling sub-code is the in-depth transient heat conduction routine; it treats two-dimensional axi-symmetric bodies using the explicit finite-difference method. It is coupled to a completely general thermochemistry sub-code for the surface state and ablation computation. This routine allows for full equilibrium considering a large number of species, and can also account for any number of non-equilibrium effects. The code also features automatic coupled calculations of the pressure around the body, using a variation of modified Newtonian relations coupled to Prandtl-Meyer expansions. The subsonic region pressure description includes empirical corrections necessary on very blunt bodies. In addition, the code automatically computes the boundary layer edge static enthalpy, the recovery enthalpy, and the convective transfer coefficient, employing appropriate computed property values for any edge gas.

TABLE OF CONTENTS

LIST OF FIGURES

LIST OF SYMBOLS

A	area of side of nodal box	ft^2
A^*_{ii}	a ratio of collision integrals based on a Lennard-Jones intermolecular potential (see Ref. 3)	---
a,b,c	nodal box side and center line lengths, Figure 7, Equation (10)	in
a_1,b_1	constants effectively defined by Equation (22)	--- and ^oR
a_2,b_2	constants in Equation (24)	$Btu/ft^2sec\ ^oR$ and Btu/ft^2sec
B_m	pre-exponential factor for kinetic reaction m (see Equation (74))	
B'	defined as $(B'_c - \sum \dot{m}_{r_\ell}/\rho_e u_e C_M)$ thermochemical ablation parameter	---
B'_c	defined as $\dot{m}_c/\rho_e u_e C_M$, total ablation parameter	---
B'_f	defined as $\sum \dot{m}_{r_\ell}/\rho_e u_e C_M$	---
B'_{tc}	same as B'	---
b	see a,b,c	
C	nodal capacity, Equation (14)	$Btu/^oF$
C_H	Stanton number for heat transfer (corrected for "blowing", if necessary)	---
C_{H_O}	Stanton number for heat transfer not corrected for blowing	---
C_{k_i}	number of k atoms in molecule i	---
C_M	Stanton number for mass transfer, corrected for "blowing", if necessary	---

SYMBOLS (continued)

C_p	specific heat capacity at constant pressure	Btu/lb ^oR
$\tilde{C}_p$	Z_i averaged heat capacity (see Equation (A-15)	Btu/lb ^oR
c	specific heat	Btu/lb ^oF
c	see a,b,c	in
D	Fick's law diffusion coefficient	ft^2/sec
$\bar{D}$	constant defined by Equation (62)	ft^2/sec
$\mathcal{D}_{ij}$	binary diffusion coefficient	ft^2/sec
E_m	activation energy for kinetic reaction m	Btu/lb mole
F	radiation view factor	---
F_i, F_j	empirical factors appearing in Equation (62)	---
$\bar{F}$	ratio of summations defined by Equation (67)	---
f	denotes general functional relationship	---
H	total enthalpy (sensible + chemical + $u^2/2$)	Btu/lb
H_r	recovery enthalpy	Btu/lb
h	static enthalpy	Btu/lb
h	heat transfer coefficient based on temperature difference	Btu/ft^2sec ^oR
h_c	enthalpy of ablating wall material at wall temperature	Btu/lb
h_w	enthalpy of gases adjacent to the wall	Btu/lb
I	total number of candidate gas phase species in the system	---
i,j	chemical species indices	---

SYMBOLS (continued)

j_i	diffusional mass flux of species i	lb i/ft^{2}sec
$\tilde{j}_k$	total diffusional mass flux of element k regardless of molecular configuration	lb/ft^{2}sec
K	total number of chemical elements in the system	---
K_i	mass fraction of species i	---
$\tilde{K}_k$	total mass fraction of element k regardless of molecular configuration	lb k/lb
K_{pi}	equilibrium constant (see Equation (39))	various
k	thermal conductivity	Btu/ft sec ^{o}R
k_{Fm}	forward reaction rate constant for kinetic reaction m (see Equation (72))	various
L	total number of candidate condensed phase species in the system	---
L	path lengths in a nodal box, Figure 5	ft
Le	Lewis number	---
ℓ^*	length scale used in heat transfer analysis, defined in Equation (126)	ft
M	Mach number	---
$\mathcal{M}$	system molecular weight $\sum x_i \mathcal{M}_i$	lb/lb mole
$\mathcal{M}_i$	molecular weight of species i	lb/lb mole
m	node corner and center row number	---
$\dot{m}$	mass flow rate per unit area from the surface thermochemical effects only	lb/ft^{2}sec
$\dot{m}_c$	total mass flow rate of "char" or main ablating material per unit surface area, all effects (thermochemical plus condensed phase mechanical removal)	lb/ft^{2}sec

SYMBOLS (continued)

$\dot{m}_{r_\ell}$	flow rate of condensed phase ℓ mechanically removed from surface	lb/ft^2sec
N	representing the molecular formula for a species	---
n	node corner and center column number	---
P	total pressure	lb/ft^2
P_i	partial pressure of species i	lb/ft^2
Pr	Prandtl number	---
q	heat flux	Btu/ft^2sec
$-q_a$	rate of energy input to solid surface by diffusional processes in the boundary layer	Btu/ft^2sec
q_{cond}	rate of energy conduction into solid material at the surface	Btu/ft^2sec
$q_{rad\ in}$	rate of energy input to the surface by radiation from the boundary layer or from outside the boundary layer, same as q_{rad}	Btu/ft^2sec
$q_{rad\ out}$	rate of energy radiated away from the surface	Btu/ft^2sec
R	thermal resistance, see Equations (17), (18)	sec $^oF/Btu$
R	universal gas constant	Btu/lb mole ^oR
R_m	net forward rate of reaction m (see Equation (72))	
R_{max}	maximum of either the nose radius R_N or R* as defined in Figure 17	ft
R_N	nose radius	ft
R*	contact thermal resistance, Equation (17); sonic point radius defined in Figure 17	$ft^2sec\ ^oR/Btu$, ft
r	radius	ft

SYMBOLS (continued)

$\tilde{r}$	recovery factor	---
S	surface location, see ΔS	ft
Sc	Schmidt number, see Equation (A-17)	---
s	entropy	Btu/lb ^{o}R
s	surface running length	ft
T	temperature	^{o}R
T_{fail}	failure or mechanical removal temperature for a surface species	^{o}R
T_w	wall (surface) temperature, general term for $T_{s,n}$	^{o}R
u	velocity	ft/sec
u*	velocity used in heat transfer analysis, defined in Equations (124)-(126)	ft/sec
V	nodal volume	ft^3
v	gas velocity normal to surface	ft/sec
X_ℓ	amount of condensed phase ℓ defined in Equation (43)	moles ℓ/ moles gas
x	streamwise location or coordinate	ft
x_j	mole fraction of species j	mol j/mol
$x_1, x_2, \ldots$	general independent variables	various
Y	variable defined in Section 4.3	Btu/lb
y	ratio defined by Equation (13)	---
y	distance normal to surface	ft

SYMBOLS (continued)

Z	axial coordinate	ft
Z_i	unequal diffusion quantity for species i, Equation (61)	---
Z_i^*	diffusion driving force see Equation (60), and (61)	---
$\tilde{Z}_k$	unequal diffusion quantity for element k regardless of molecular configuration	---
$\tilde{Z}_k^*$	unequal diffusion driving potential quantity for element k regardless of molecular configuration (see Equation (59)	---

GREEK

α	heated surface absorbtivity (taken equal to ε_w)	---
α_{kj}	mass fraction of element k in species j	lb k/lb j
β	angle between body centerline and surface normal	radians
γ	a mass fraction - Z fraction weighting exponent, see Equation (60)	---
γ	isentropic exponent	---
Δ	denotes change	---
ΔS	change in surface point location during $\Delta\theta$	---
$\Delta\theta$	time step in finite difference solution	sec
ϵ	emissivity or emittance	---
ε	error or departure from zero	various
ε	an empirical diffusion factor correlation exponent (see Equation (63))	---
η	input multiplicative safety factor in time step calculation, Equation (19)	---

SYMBOLS (continued)

θ	time	sec
θ	angle between velocity vector and a line normal to a shock	radians
λ	constant in Equation (128)	---
λ	dimensionless length ratio defined by Equations (90) and (96)	---
μ	dynamic viscosity	lb/ft sec
μ_{jm}	stoichiometric coefficient for species j of kinetic reaction m (see Equation (72))	---
μ_1, μ_2, μ_3	quantities defined by Equations (A-4), (A-5), and (A-14), respectively	--- and lb/lb mol; lb mol/lb
ρ	density	lb/ft^3
$(\rho v)_w$	$\dot{m} = \dot{m}_c - \sum \dot{m}_{r_\ell}$	lb/ft^{2}sec
$\rho_e u_e$	mass flow at boundary layer edge	lb/ft^{2}sec
$\rho_e u_e C_H$	heat transfer convective film coefficient	lb/ft^{2}sec
$\rho_e u_e C_M$	mass transfer convective film coefficient	lb/ft^{2}sec
σ	Stefan-Boltzmann constant	Btu/ft sec $^\circ R^4$
$\varphi, \bar{\varphi}$	energy thicknesses defined by Equation (105) and (106)	ft
φ	parameter defined by Equation (127)	---
ϕ_m	temperature exponent in the rate coefficient for kinetic reaction m (see Equation (74))	---

SUBSCRIPTS

A,B,C,D	indices for path lengths L (Figure 5), nodal s side areas A (Figure 6) and thermal resistances R (Figure 10)
a	see q_a

SYMBOLS (continued)

a,b,c	denote side lengths, Figure 7
B	see A,B,C,D
bw	denotes back wall, comunicating with reservoir
C	see A,B,C,D
CL	denotes nodal column center line
c	denotes nodal box corner
c	denotes total amount of "char" or ablating material; see $\dot{m}_c$
D	see A,B,C,D
e	denotes boundary layer outer edge, or boundary layer edge gas
FD	denotes flat disc
fail	refers to material failing (being removed) from heated durface in condensed phase, e.g., mechanical removal, melting
g	denotes gas phase
H	see C_H
i	station index
i,j	denotes any identifiable species: atom, ion, molecule (i reserved for gas phase)
int	internal contribution to thermal conductivity, Equation (A-9), (A-12)
k	denotes element
ℓ	index of condensed phase species mechanically removed from surface

SYMBOLS (continued)

M	see C_M
M	match point
m	general index
m	node corner and center row number index
mix	refers to total mixture property, Equation (A-9)
mono	refers to pure species, Equations (A-10), (A-11)
mono-mix	refers to simplified mixture rule, Equation (A-10)
N	denotes node center
N	see R_N
n	node corner and center column number index
r	see $\dot{m}_{r_\ell}$
r	denotes recovery, radiation
rad	see $q_{rad\ in}$, $q_{rad\ out}$
ref	refers to an empirical reference value of molecular weight, Equation (63)
res	"reservoir" communicating with back wall
s	denotes heated surface
t	total; transition point
w	denotes wall, i.e., heated surface
o	see C_{H_O}
1,2	see x_1,x_2; also denote "earlier" and "later"

SYMBOLS (concluded)

θ,θ'	at times θ and θ', respectively
∞	denotes free stream condition

SUPERSCRIPTS

'(prime)	see B', B'_c, B'_f, B'_{tc}
'(prime)	denotes at new time $\theta' = \theta + \Delta\theta$
'(prime)	at the reference enthalpy
P	reaction products
R	reaction reactants
T_w	enthalpy datum temperature - wall temperature
–	normalized by stagnation point pressure; also see $\bar{D}$, $\bar{F}$, $\bar{\varphi}$
~	denotes total appearance of element independent of molecular configuration
*	sonic point
*	see $\tilde{Z}_k^*$, Z_i^*, R*
*	x_i^* denotes the current estimated value of the variable x_i during an iterative solution
**	x_i^{**} denotes the new estimated value of the variable x_i during an iterative solution
	see $\dot{S}$

SECTION 1

GENERAL INTRODUCTION

1.1 PROBLEM STATEMENT

1.1.1 Background

The computation of the thermal and dynamic history of a vehicle entering a planetary atmosphere has a number of important features, which may be crudely summarized as follows:

I. Trajectory analysis
II. Inviscid flow field calculation
III. Boundary layer calculation
IV. Interactions between vehicle surface and boundary layer
V. In-depth response

Complete calculation of vehicle response over a period of time would involve a coupled calculation of all five phases, each computation phase providing, in effect, the time dependent boundary conditions for the adjacent phases.

A recent survey (Ref. 1) has carefully examined the current computational state-of-the-art for each phase and for the coupling between phases. Major deficiencies were identified in Phase III, boundary layer calculations, where general solution procedures for reacting multicomponent boundary layers did not exist, in Phase IV, where sufficiently general chemical routines did not exist, and in Phase V, where multidimensional in-depth solution programs did not exist. In addition, no III-IV-V coupled programs existed. Programs with IV-V coupling existed, but were limited to one space dimension for the in-depth response.

Efforts to upgrade the computational state-of-the-art will probably not attempt to couple together large "complete" computer routines for all of the five phases; the resulting computer code would be unwieldly, uneconomical, and unreliable. Since, in general, the coupling aspects of the predictive problem are more interesting and important than the degree of computational detail in the individual phases, a more judicious computational approach seeks to couple detailed calculations of only one or perhaps two problem phases to less detailed approximate or correlation calculations of several of the other phases. The resulting computer code would include the important coupling effects without becoming excessively large, and would still offer good detail in at least one phase of the total problem.

1.1.2 Present Computer Code

The work reported here exemplifies this latter approach. The code developed under this program includes large subroutines for the detailed computation of the transient in-depth temperature response of an ablating heat shield (Phase V in the scheme above) and also of the thermochemical interactions between the environment gas and the heated surface of the heat shield material (Phase IV). The program features more simplified approaches for the boundary layer transport calculations (Phase III), for which a convective transport coefficient approach was adopted, and for the inviscid flow field calculations (Phase II), for which empirical correlation and various modifications of Newtonian pressure distributions are used to find the pressure around the ablating body. These combine with the isentropic expansion assumption to define the boundary layer edge state.

The completed code may thus be termed a "II - III - IV - V coupled code", in which the routines for phases IV and V are relatively complete, general, and large, while those for phases II and III are relatively small and simplified. The nature of the individual phase routines may be summarized as follows:

Phase	Code Characteristics
Phase V - In-Depth Response	2-D Axisymmetric Finite Difference Transient Heat Conduction Code, Explicit, Multi-material Capability, General Geometry but some restrictions on grid layout make use on very sharp bodies difficult, non-charring materials, some types of anisotropy considered
Phase IV - Surface Response	General thermochemical state routine allows for ablation of any one material in any environment, considers full equilibrium plus any number of heterogeneous and homogeneous (but surface area scaled) kinetically controlled reactions; identifies thermochemically controlling surface material, detects failing or melting compounds

Phase	Code Characteristics
Phase III - Boundary Layer	Transfer Coefficient routine based on energy integral technique, laminar only at present time, boundary layer radiation not evaluated
Phase II - Flow Field	Modified Newtonian pressure for sharp bodies, blending into empirical pressure correlations for blunt bodies combined with Prandtl-Meyer expansions for supersonic regions; isentropic expansion used for boundary layer edge and recovery state calculations, flow field radiation not evaluated
Phase I - Trajectory	Not included in program, time histories of stagnation pressure and enthalpy to be input

1.1.3 Purpose of This Report

This report presents a description of the coupled code. It describes the general nature of the code and the flow of information from one computation phase to the other. The report also describes the physical models used in each computational phase, and outlines in some detail the numerical analysis used in each phase. The report does not include a users guide; this has been published separately (Reference 2).

SECTION 2

OVERVIEW OF COMPUTER PROGRAM AND REPORT

Figure 1 illustrates the general physical problem considered by the code.

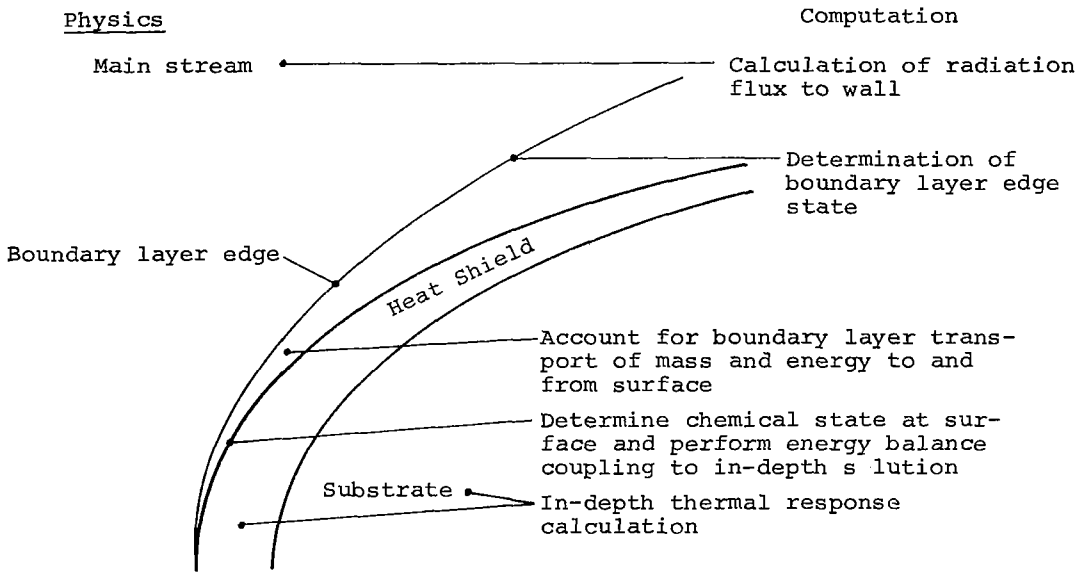

Figure 1. Sketch of Problem Considered

In the coupled code, the routine for the in-depth thermal response calculations (Phase V) functions as the main, controlling routine. It is referred to as MACABRE, after "Material Ablation with Chemically Active Boundary Layers in Re-Entry". The coupling between Phases V and IV effected through the surface energy balance calculation, which is performed by a separate subroutine, SURFB. This energy calculation naturally requires (among other things) information about the enthalpy of the boundary layer gases adjacent to the wall; this information is called for by SURFB when needed and obtained from a package of complex thermochemistry subroutines controlled by subroutine EQUIL. In addition, SURFB requires values for a convective transfer coefficient, obtained as needed from subroutine RUCH, for the local pressure, obtained as needed from subroutine RUNLP, and for the local recovery enthalpy, obtained as needed from subroutine PARBL. Calls to PARBL, RUNLP, and RUCH constitute IV - III - II coupling, filling out the coupling requirements of the code.

Sections 3 through 9 below describe the various computational phases and the coupling links between them. This necessarily involves much detail. Section 10 then presents a recapitulation of this introductory section and some overall flow charts of the computer code operations which should illustrate more clearly all of the important features of the program.

SECTION 3

IN-DEPTH TRANSIENT THERMAL CALCULATION

3.1 GENERAL REMARKS

The in-depth transient temperature calculation serves as the controlling logic unit for the entire coupled computer code. (It also consumes most of the computing time.) This calculation is of the familiar finite difference, lumped-capacity type. The following sections describe the nodal grid employed for this calculation and the basic equations employed.

3.2 NODAL LAYOUT AND GEOMETRY

3.2.1 General Pattern

The geometric shape considered, illustrated in Figure 2, is imagined to be divided up into a grid pattern in the customary manner for finite difference computation schemes. The area within each grid "box" will be termed a "node"; this is in contrast to terminology which calls each corner of the grid network a node. The thermal capacity of each node is imagined to be lumped at a single point within the box; this point will be termed the nodal center. It will be convenient to assume for the moment that the nodal center may be located anywhere within the nodal box. Strategies for optimizing the location of the nodal centers will be discussed later.

For convenience, the nodes are imagined to be quadrilaterals, so that the entire nodal network is an assemblage of quadrilaterals. For bookkeeping

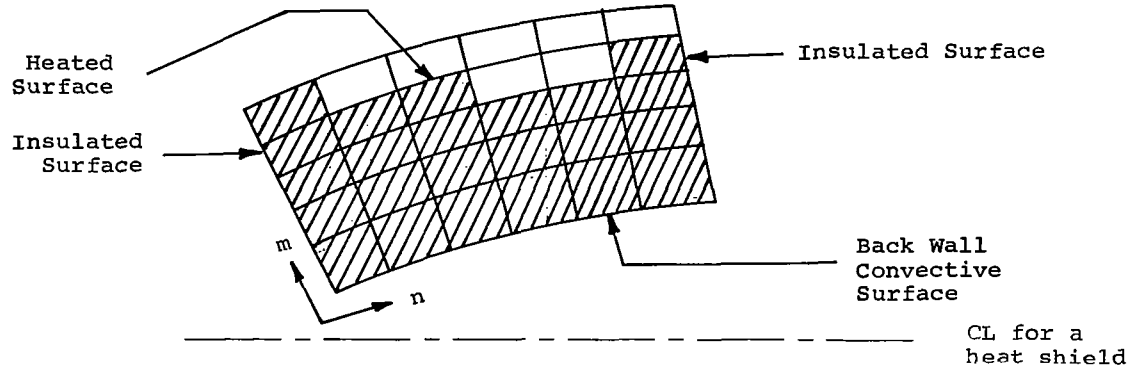

Figure 2. Sketch of Typical Nodal Layout

convenience, the network is imagined to be "complete", even though the shape of the material may dictate that some of the mesh boxes are empty. Both nodes (boxes or centers) and mesh corners are numbered in a row and column system which will be labeled as an m-n system, where m denotes a row and n denotes a column. The m-n mesh scheme may be oriented arbitrarily with respect to the physical r-Z coordinate scheme,* so that in general the row-column description might seem to be merely a descriptive artifice; however, in exploiting the simplicities associated with low curvature bodies and heat shields it has been assumed in constructing the program that the heated surface is at the top of the columns, as indicated in Figure 2. Thus as surface recession occurs, the boxes at the top of each column shrink; the other boxes remain fixed. This limitation that the heated surface be located at the top of each column is merely a convenience procedure exploited for the special case of heat shields typical of fairly blunt cones. For high curvature bodies such as sharp cones this restriction becomes inconvenient, although Reference 2 gives an example of the successful use of the code on a very sharp body.

The side walls of the nodal network are presumed insulated and the back wall communicates through a simple heat transfer coefficient law (plus radiation) to a "reservoir" at T_{res}. Thus the boundary condition at this face does not involve thermochemistry.

Three other "convenience limitations" have been applied to the layout of the nodal grid. First, it is assumed for the purposes of computing thermal conductances between nodal centers that the mesh scheme is nearly orthogonal, so that conductance may be taken as conductivity times side-area divided by length.** Secondly, it is presumed that only one material ablates, and that only one material is exposed to the heated surface. Thirdly, it is presumed that the principal directions of thermal anisotropy are aligned with the nodal mesh. This simplifies computations and reduces input requirements. For those applications in which the heated surface intersects the principal directions of anisotropy at "difficult" angles this restriction could become a major inconvenience and more general schemes would have to be devised for those problems.

---

*That is, the nodal mesh scheme may be above or below the Z-axis line, may be oriented in any general direction, and may be "bent" or shaped in any manner convenient to the user (subject to the limitations described in the paragraphs following below).

**A suitable more general conductance calculating scheme could remove this restriction without any essential change to the program.

3.2.2 Geometry

3.2.2.1 Location of Nodal Centers

The study summarized in Reference 3 showed that to obtain a node dropping scheme which produce smooth surface temperature histories, it was necessary to avoid associating thermal capacity with the surface temperature. In terms of the conventional thermal RC network, this means that a one-dimensional scheme would look like Figure 3. All the capacity

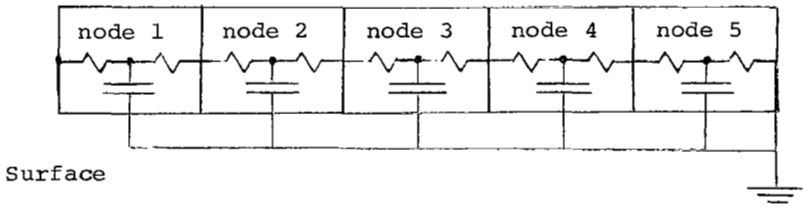

Figure 3. Sketch of One-Dimensional Thermal RC Network

of the surface node is located in the center of the first nodal zone, and half of the thermal resistance of this zone is interposed between the surface temperature and the temperature of the first capacity lump. Note that for m nodes or boxes the system has m+1 temperature points, in contrast to most schemes.* Thus for an m x n nodal network scheme, there will be m x n nodal temperatures (associated with thermal capacity) plus n surface temperatures (not associated with thermal capacity).

Denoting the nodal center coordinates as r_N and Z_N, the coordinates for node m, n with corner coordinates as shown in Figure 4 may be represented in terms of the corner coordinates by Equations (1) and (2):

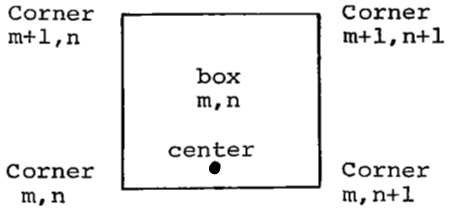

Figure 4. Sketch of Nodal Center Location For Ablating Material

*The capacity location scheme described here is an improvement over that recommended in Reference 3.

$$r_{N,m,n} = \frac{r_{c,m,n} + r_{c,m+1,n} + r_{c,m+1,n+1} + r_{c,m,n+1}}{4} \quad (1)$$

$$z_{N,m,n} = \frac{z_{c,m,n} + z_{c,m+1,n} + z_{c,m+1,n+1} + z_{c,m,n+1}}{4} \quad (2)$$

(Nodes in the ablating material will automatically be centered*; the MACABRE user has the option to put back-up material nodal centers anywhere in the nodal box.)

3.2.2.2 Path Lengths for Conduction

In this and the following sections, the nodal center will have a general location $r_{N,m,n}$, $z_{N,m,n}$ for illustrative purposes. For computing thermal conductances, it will be necessary to have thermal path lengths between nodes. Since material properties are associated with each nodal box, it is convenient first to consider path segments inside each box. In general there are four path segments of interest as shown in Figure 5. The program computes the lengths $L_{m,n,B}$

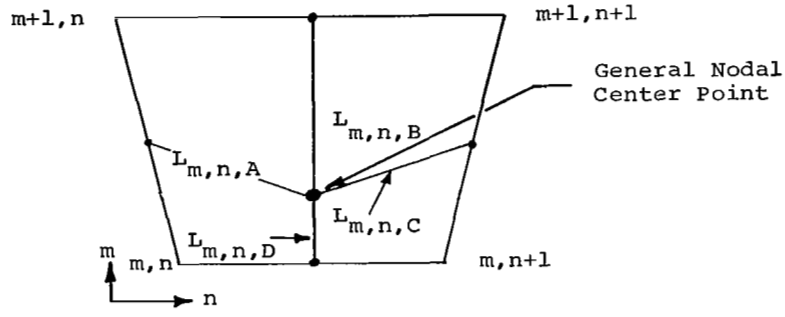

Figure 5. Illustration of Path Lengths

and $L_{m,n,D}$ in the m direction as the distances between the nodal center and the centers of the m+1 and m faces of the box. (This is because the nodal center is usually on the line joining the centers of these two faces.) Thus the paths B and D have the lengths

*Except for the first column, in which nodal points are centered on the first side of the box (between corners m,1 and m+1,1) under the assumption that this line of sides will end at the body stagnation point.

$$L_{m,n,B} = \left[\left(\frac{r_{c,m+1,n} + r_{c,m+1,n+1}}{2} - r_{N,m,n}\right)^2 + \left(\frac{Z_{c,m+1,n} + Z_{c,m+1,n+1}}{2} - Z_{N,m,n}\right)^2\right]^{\frac{1}{2}} \quad (3)$$

$$L_{m,n,D} = \left[\left(\frac{r_{c,m,n+1} + r_{c,m,n}}{2} - r_{N,m,n}\right)^2 + \left(\frac{Z_{c,m,n+1} + Z_{c,m,n}}{2} - Z_{N,m,n}\right)^2\right]^{\frac{1}{2}} \quad (4)$$

Similarly, for the n direction path lengths

$$L_{m,n,A} = \left[\left(\frac{r_{c,m,n} + r_{c,m+1,n}}{2} - r_{N,m,n}\right)^2 + \left(\frac{Z_{c,m,n} + Z_{c,m+1,n}}{2} - Z_{N,m,n}\right)^2\right]^{\frac{1}{2}} \quad (5)$$

$$L_{m,n,C} = \left[\left(\frac{r_{c,m+1,n+1} + r_{c,m,n+1}}{2} - r_{N,m,n}\right)^2 + \left(\frac{Z_{c,m+1,n+1} + Z_{c,m,n+1}}{2} - Z_{N,m,n}\right)^2\right]^{\frac{1}{2}} \quad (6)$$

3.2.2.3 Side areas

Areas of the sides of each box are also required for thermal conductance calculations. For the sides lettered as shown in Figure 6, the areas are

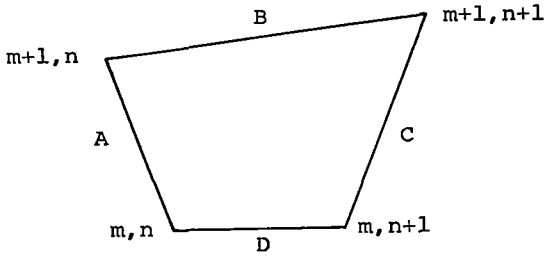

Figure 6. Nomenclature of Nodal Sides

given by elementary geometry (First Theorem of Pappus)

$$A_{m,n,A} = \pi(r_{c,m,n} + r_{c,m+1,n})\left[(r_{c,m+1,n} - r_{c,m,n})^2 + (Z_{c,m+1,n} - Z_{c,m,n})^2 \right]^{\frac{1}{2}} \quad (7)$$

$$A_{m,n,B} = \pi(r_{c,m,n} + r_{c,m,n+1})\left[(r_{c,m,n+1} - r_{c,m,n})^2 + (Z_{c,m,n+1} - Z_{c,m,n})^2 \right]^{\frac{1}{2}} \quad (8)$$

Only these two areas need to be computed for each box, since the areas on the other sides of the nodal box are identical with the areas A and B of adjacent nodes.

3.2.2.4 Volume

The volume of the elemental box is by the Second Theorem of Pappus,

$$\begin{aligned} V_{m,n} = \Big[\pi/3 \Big\{ & Z_{c,m,n}\left[r_{c,m,n}(r_{c,m,n+1} - r_{c,m+1,n}) + r^2_{c,m,n+1} - r^2_{c,m+1,n} \right] \\ & + Z_{c,m+1,n}\left[r_{c,m+1,n} \cdot (r_{c,m,n} - r_{c,m+1,n+1}) + r^2_{c,m,n} - r^2_{c,m+1,n+1} \right] \\ & + Z_{c,m+1,n+1}\left[r_{c,m+1,n+1}(r_{c,m+1,n} - r_{c,m,n+1}) + r^2_{c,m+1,n} - r^2_{c,m,n+1} \right] \\ & + Z_{c,m,n+1}\left[r_{c,m,n+1} \cdot (r_{c,m+1,n+1} - r_{c,m,n}) + r^2_{c,m+1,n+1} - r^2_{c,m,n} \right] \Big\} \Big] \end{aligned} \quad (9)$$

3.2.2.5 *Geometric Effects of Surface Recession*

For nodes adjacent to the heated surface, side B may move due to surface recession (ablation). This recession reduces the thermal resistance between the surface point and the adjacent nodal point, increases transverse thermal resistances (as discussed below), and reduces the thermal capacity associated with the nodal center of the nodal box adjacent to the surface.

The program assumes that the surface recession occurs so as to maintain the ratios

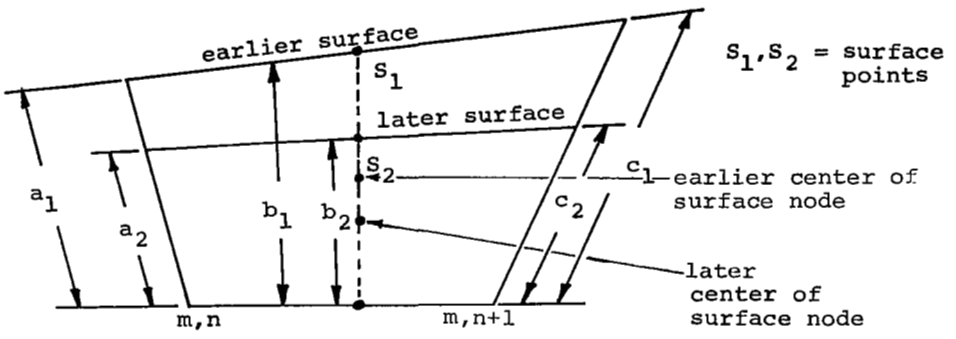

Figure 7. Sketch of Surface Nodal Box Undergoing Recession

$$\frac{a_2}{a_1} = \frac{b_2}{b_1} = \frac{c_2}{c_1} \tag{10}$$

as shown in Figure 7. The b line joins the centers of the m+1 and m planes and serves to define the location of the surface point S*. The moving corners m+1,n and m+1, n+1 are located accordingly, and the areas and volumes computed as before, except that for these nodes $A_{m,n,A} \neq A_{m,n-1,C}$.

The nodal point or center is also presumed to move so that is is always in the arithmetic center of the nodal box*. Thus the nodal center is "squeezed" toward the back wall of the nodal box as recession proceeds. The path lengths for conduction are adjusted accordingly.

3.2.2.6 Surface Shape

As noted above and illustrated by Figure 7, it is most convenient to consider the surface points on the heated surface as being always located on the nodal column center line*, that is, on the line joining the center points of the m+1 and m planes ("parallel" to the heated surface), where m is the row index of a nodal box at the surface and m+1 is the local corner index of the heated surface (see Fig. 7). The location of the surface points is all the information needed about the surface for those ablation problems with a specified, input surface recession rate as a boundary condition (the various ablation problem boundary condition options are described in Section 4 below), since for those problems it is most convenient to specify, as input, recession history along the nodal center line. The nodal grid as input thus serves

*Except, as noted above, for the first column of nodal boxes, in which the nodal points are centered on the first side (Side A of Figure 6) of the nodal box and the surface point S is located at the corner m+1,1 (Figure 7).

to define the various nodal column center lines, and the recession history for each column then defines the history of the surface points in a perfectly straightforward manner. However, another important heated surface boundary condition option involves not input recessions but various energy and chemistry information sufficient to calculate surface mass loss from energy balance considerations (Option 1, discussed in Section 4.3 below). This ablation calculation does not produce recession rates directly, of course; instead it produces rates of mass loss from the surface. It will prove convenient, nevertheless, to adhere to the concept of the surface point which moves along the column center line as recession progresses. To define the surface point motion with computed mass loss rates determined from this general energy-balance-determined option requires knowledge of the angle between the local normal to the surface and the column center line, since computed mass loss may be translated directly into recession along a normal to the surface. Recession along the normal may be projected into the nodal column center line once the angle between these two lines is known. The direction of the surface normal may conveniently be determined from the slope of the surface, that is the surface shape, and of course the direction of the column center line is known.

It is obviously not safe to use the slope of the heated (top) surface of the surface nodal box to obtain the surface slope, since in general it is neither possible nor always desirable to lay out a nodal grid which will "conform" to the "real" surface for the entire problem history. Therefore the MACABRE program includes various special curve-fit subprograms which compute a surface shape at each time step during the solution after examining the layout of the surface points. Referring to Figure 8, one curve fit subprogram program computes the

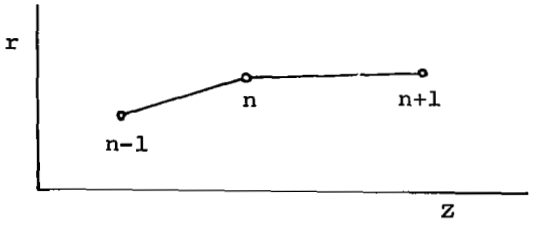

Figure 8. Sketch of Surface Points

slope of the surface, dr/dZ, at surface point n as the average of the slopes between surface points n-1 and n, and n and n+1. Thus

$$\left.\frac{dr}{dZ}\right|_n = \frac{1}{2}\left(\frac{r_n - r_{n-1}}{Z_n - Z_{n-1}} + \frac{r_{n+1} - r_n}{Z_{n+1} - Z_n}\right) \qquad (11)$$

Note that n-1, n, and n+1 are surface points, not nodal corner points. (Problems with only one nodal column have only one surface point. This requires the program to abandon the average slope scheme and to use the nodal box heated surface slope as the surface slope.)

Other curve fit routines are available which involve fitted quadratics in successive intervals. The User's Manual gives recommendations for the choice of fit routines for different body shapes.

Special formulas are used for the slopes at the first and second surface points, however, in order to harmonize the array of surface slope values with some basic assumptions made in the convective transfer coefficient routines. Since the first column surface point is presumed to be the stagnation point, the slope here is set to a very large positive value. It is assumed that the surface is spherical between the first and second points, so that the second point surface slope is given by

$$\left.\frac{dr}{dz}\right|_2 = \frac{1 - y^2}{2y} \tag{12}$$

where

$$y = \frac{z_2 - z_1}{r_2} \tag{13}$$

With surface slope determined, the surface movement ΔS computed during the time step may be projected onto the nodal box center line, and then the

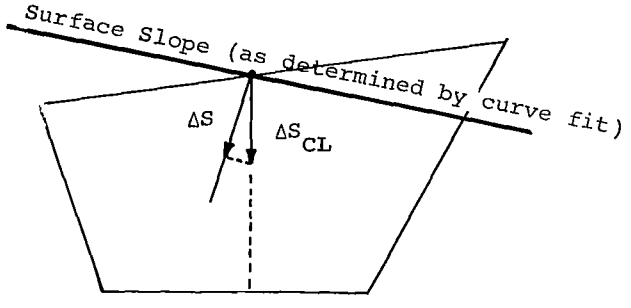

Figure 9. Sketch of Surface Geometrical Relationships (exaggerated)

new nodal volume computed, as indicated in the exaggerated sketch of Figure 9. Actual surface movement during a time step is limited to a small fraction of the nodal thickness to ensure a good approximation to the conservation of mass. Note again that the first column is an exception, since the surface point is located on the left corner, not in the center of the top surface.

3.3 INTERNAL CONDUCTION PARAMETERS

The thermal resistances between nodes and the thermal capacity of the nodes are calculated each time interval from the material properties of the node corresponding to its temperature at that time. The material properties (density (ρ), specific heat (c), conductivity (k), and emissivity (ε) are input as table look up functions of temperature. Linear interpolation is employed for material property determination at temperatures intermediate to those tabulated. Constant thermal contact resistances may be specified between any or all nodes. The nodal capacities and resistances are calculated as follows:

$$C_{m,n,\theta} = \rho_{m,n,\theta} c_{m,n,\theta} V_{m,n} \tag{14}$$

$$R_{m,n,A,\theta} = \frac{1}{A_{m,n+1,A}} \left(\frac{L_{m,n,C}}{k_{m,n,\theta}} + \frac{L_{m,n+1,A}}{k_{m,n+1,\theta}} + R^{*}_{m,n,B} \right) \tag{15}$$

$$R_{m,n,B,\theta} = \frac{1}{A_{m+1,n,B}} \left(\frac{L_{m,n,B}}{k'_{m,n,\theta}} + \frac{L_{m+1,n,D}}{k'_{m+1,n,\theta}} + R^{*}_{m,n,A} \right) \tag{16}$$

Figure 10 shows the locations of resistances $R_{m,n,A,\theta}$ and $R_{m,n,B,\theta}$. The

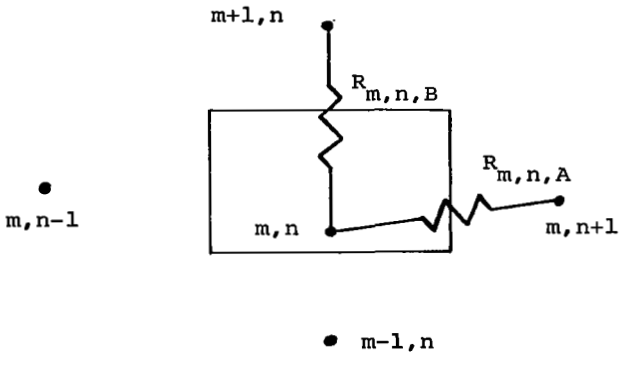

Figure 10. Sketch of Thermal Resistance Nomenclature

resistances on the other two sides of the nodal box are calculated when the quantities for the adjacent nodes are calculated. For nodes adjacent to the surface, however, $A_{m,n,C} \neq A_{m,n+1,A}$ generally (refer to Fig. 6 for area nomenclature); for these nodes

$$R_{m,n,A} = \frac{L_{m,n,C}}{A_{m,n,C}k_{m,n,\theta}} + \frac{L_{m,n+1,A}}{A_{m,n+1,A}k_{m,n+1,\theta}} + \frac{R^*_{m,n,B}}{A_{m,n,C}} \qquad (17)$$

It should be noted that anisotropic thermal conductivity values k and k' are used in Equations (15) and (16), respectively.

3.4 IN-DEPTH CONDUCTION SOLUTION

The in-depth conduction solution is the explicit finite difference type often employed for transient heat conduction analysis. The temperature of node m,n at time θ' ($T_{m,n,\theta'}$) is obtained by application of the finite difference energy balance and rate equations to the nodal volume.

Solving for $T_{m,n,\theta'}$, one obtains

$$T_{m,n,\theta'} = \left[\frac{T_{m+1,n,\theta}}{R_{m,n,B,\theta}} + \frac{T_{m,n+1,\theta}}{R_{m,n,A,\theta}} + \frac{T_{m-1,n,\theta}}{R_{m-1,n,B,\theta}} + \frac{T_{m,n-1,\theta}}{R_{m,n-1,A,\theta}} - T_{m,n,\theta} \cdot \left(\frac{1}{R_{m,n-1,A,\theta}} + \frac{1}{R_{m,n,B,\theta}} + \frac{1}{R_{m,n,A,\theta}} + \frac{1}{R_{m-1,n,B,\theta}}\right)\right] \frac{\Delta\theta}{C_{m,n,\theta}} + T_{m,n,\theta} \qquad (18)$$

In the program this equation is used to obtain "new" temperatures for all nodes except for two nodes in each column adjacent to the heated surface and for back wall nodes. The nodes near to the heated surface are linked to the surface temperature implicitly and hence a special procedure is used for the temperature of these nodes, as described in the next section.

Back wall nodes include a quantity

$$hA_{m,n,D}(T_{res} - T_{m,n,\theta}) + \sigma\epsilon_{bw}A_{m,n,D}(T^4_{m,n,\theta} - T^4_{res})$$

inside the brackets of Equation (18), and have $T_{m-1,n,\theta}$ formally equal to zero.

The explicit relation (18) imposes the familiar stability restriction on the time step size $\Delta\theta = \theta' - \theta$. The MACABRE program automatically employs a conservative stability equation for interior nodes:

$$\Delta\theta = \eta\left[\frac{C_{m,n}}{\frac{1}{R_{m,n,A}} + \frac{1}{R_{m,n,B}} + \frac{1}{R_{m,n-1,A}} + \frac{1}{R_{m-1,n,B}}}\right] \qquad (19)$$

Normally for stability, the input parameter η is less than unity. Surface nodes are not considered for time interval calculation, as will be explained below; back wall nodes include the terms $A_{m,n,D}(h/2 + 4\sigma\varepsilon_{bw}T^3_{m,n,\theta})$ in the denominator.

The automatic stability criterion calculation may be suppressed for any node if the user is sure that the allowed time step for that node will never be the minimum one for the system. This saves some computer time.

Alternatively, the stability criterion calculation can be suppressed entirely. If it is not used, then $\Delta\theta$ must be specified.

3.5 TEMPERATURES OF SURFACE NODES AND SURFACE POINTS

Temperatures of surface points are determined either by assignment (Option 2) or by surface energy balances described in the next section (Options 1 and 3). The surface energy balance determines the new surface temperature of the nth column T'_{s_n} with an implicit iteration technique. Stability considerations dictate that the first and second node temperatures also be treated implicitly, and that any transverse heat conduction link (across columns) for surface temperatures must be implicit. This latter requirement is a complex one to meet as columns recede; hence the surface temperature points are not linked transversely. Figure 11 shows the implicit and explicit heat conduction paths for two typical situations.

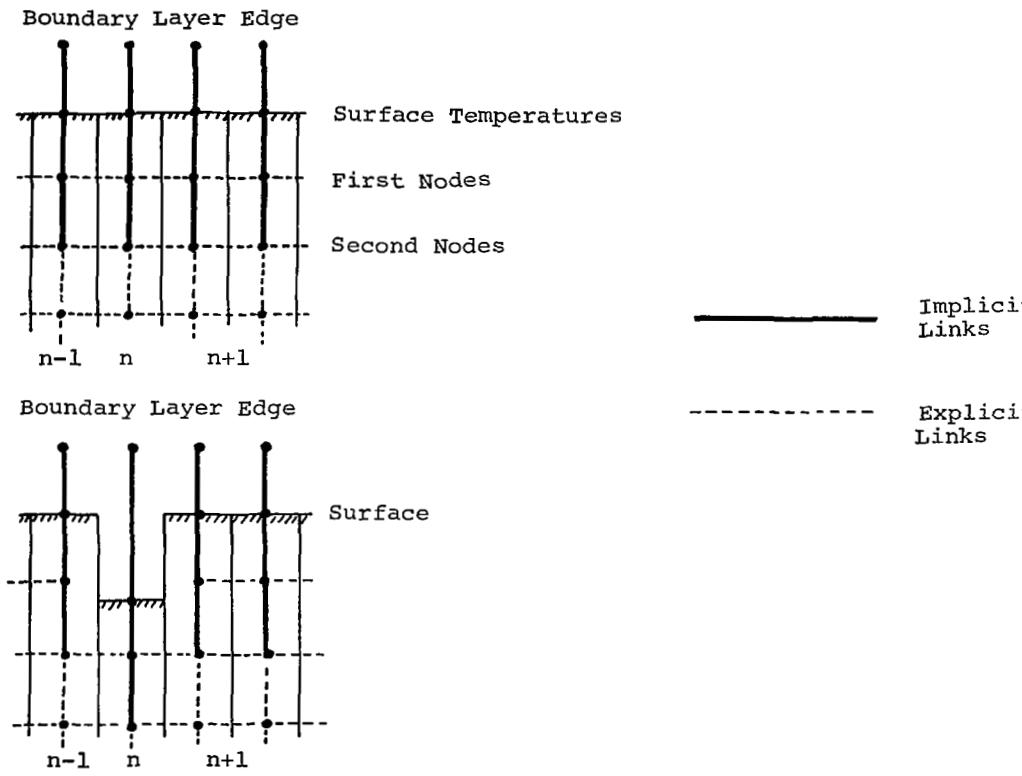

Figure 11. Sketch of Implicit and Explicit Temperature Links in Finite Difference Solution, for Two Typical Situations

In general terms, the equation for the new temperature of a surface node (not a surface point) is

$$T_{m,n,\theta'} = \left[\frac{T_{m,n+1,\theta} - T_{m,n,\theta}}{R_{m,n,A,\theta}} + \frac{T_{m,n-1,\theta} - T_{m,n,\theta}}{R_{m,n-1,A,\theta}} + \frac{T_{m-1,n,\theta'} - T_{m,n,\theta'}}{R_{m-1,n,B,\theta}} + \frac{T_{s,n,\theta'} - T_{m,n,\theta'}}{R_{m,n,B,\theta}} \right] \frac{\Delta\theta}{C_{m,n,\theta}} + T_{m,n,\theta} \quad (20)$$

This equation links the new first node temperature $T_{m,n,\theta'}$ and to the new temperature of the next node down $T_{m-1,n,\theta'}$. Another equation also links

$T_{m,n,\theta'}$ and $T_{m-1,n,\theta'}$; this is the energy balance on the second node down. This has the same form as Equation (18) with $T_{m,n,\theta}$ and $T_{m-1,n,\theta}$ replaced by $T_{m,n,\theta'}$ and $T_{m-1,n,\theta'}$ in the conductance terms:

$$T_{m-1,n,\theta'} = \left[\frac{T_{m-1,n+1,\theta} - T_{m-1,n,\theta}}{R_{m-1,n,A,\theta}} + \frac{T_{m+1,n-1,\theta} - T_{m-1,n,\theta}}{R_{m-1,n-1,A,\theta}} + \frac{T_{m-2,n,\theta} - T_{m-1,n,\theta}}{R_{m-2,n,B,\theta}} + \frac{T_{m,n,\theta'} - T_{m-1,n,\theta'}}{R_{m-1,n,B,\theta}} \right] \frac{\Delta\theta}{C_{m-1,n,\theta}} + T_{m-1,n,\theta} \qquad (21)$$

Equations (20) and (21) between them have three new unknown temperatures at each time step: $T_{s,n,\theta'}$, $T_{m,n,\theta'}$, and $T_{m-1,n,\theta'}$ (where m here denotes the row index of the surface nodal box in Column n). The two equations may be combined to eliminate $T_{m-1,n,\theta'}$, leaving a simple linear link between the surface point temperature $T_{s,n,\theta'}$ and the surface node temperature $T_{m,n,\theta'}$. Formally we have a relation between the two unknowns as

$$T_{m,n,\theta'} = f(T_{s,n,\theta'}) = a_1 T_{s,n,\theta'} + b_1 \qquad (22)$$

The surface energy balance has the general form (as described in the next section)

convection and chemical energy terms $(T_{s,n,\theta'})$

+ radiation to wall - radiation out $(T_{s,n,\theta'})$

$$= \frac{T_{s,n,\theta'} - T_{m,n,\theta'}}{A_{m,n,B,\theta}} R_{m,n,B,\theta} = q_{cond} \qquad (23)$$

where the parentheses denote functional relationship. The equation is written on a unit area basis. Relation (22) may be substituted into Equation (23) to give the non-linear surface energy balance Equation for $T_{s,n,\theta'}$:

convection and chemical energy terms $(T_{s,n,\theta'})$

+ radiation to wall - radiation out $(T_{s,n,\theta'})$

$$= a_2 T_{s,n,\theta'} + b_2 = q_{cond} \qquad (24)$$

When $T_{s,n,\theta'}$ has been found from this equation, the new surface node temperature $T_{m,n,\theta'}$ may be found from Equation (22). For surface energy balance options, the method for finding $T_{s,n,\theta'}$ is described in Section 4 below. (In Option 2, $T_{s,n,\theta'}$ is known immediately by user assignment and Equations (20) and (21) then determine $T_{m,n,\theta'}$ and $T_{m-1,n,\theta'}$ at once.)

SECTION 4

IV-V COUPLING TO SURFACE THERMOCHEMISTRY SOLUTION

4.1 GENERAL ASPECTS

The direct computational link between the subsurface solution and the surface state solution is effected through the surface energy balance calculation.* This linkage was discussed from the point of view of the in-depth solution in Section 3 above and the energy equation written down in schematic terms as Equations (23) and (24). We now must discuss this equation in more detail. The energy balance is illustrated in Figure 12,

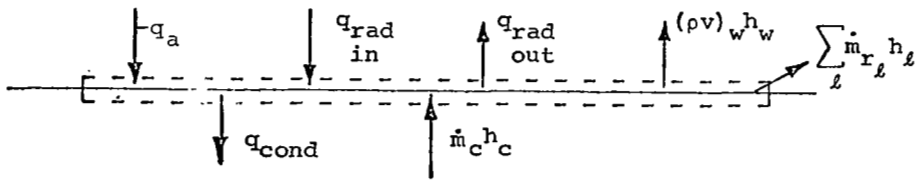

Figure 12. Representation of Surface Energy Terms During Ablation

where the indicated control volume is fixed to the receding surface. Energy fluxes leaving the control volume include conduction into the material, radiation away from the surface, energy in any flow of condensed phase material such as mechanical removal, and gross blowing at the surface. Energy inputs to the control volume include radiation in from the boundary layer and enthalpy flux due to the char flow rate. The final input in the sketch is denoted $-q_a$. It includes all diffusive energy fluxes from the gas-phase boundary layer. If the in-depth response computation were coupled to an exact boundary-layer solution, the term $-q_a$ would be obtained from that solution procedure and is, of course, a complex function of the boundary-layer structure. If, on the other hand, the in-depth response is being coupled to a simplified boundary-layer scheme such as a convective film coefficient model, as will be done here, then the term $-q_a$ assumes the form of a correlation equation.

The computation of the surface energy balance requires from the in-depth solution a relation between the surface temperature and the rate of energy conduction into the material, q_{cond}. As noted in Section 3 above, this relation derives naturally from the finite difference energy balance for the

*For Option 1 calculations. The simpler surface options will be discussed in Sections 4.5 and 4.6 below.

the node just under the surface and is a simple linear equation $q_{cond} = a_2 T_w + b_2$. With this information, the surface energy balance considerations allow determination of the thermochemical erosion rate $\dot{m}_c$ and surface temperature T_w. Itwill be useful to keep in mind that, from this point of view, the purpose of the in-depth solution at any instant is to provide information about $q_{cond}(T_w)$. The surface energy balance equation may be written as

$$-q_a + q_{\substack{rad \\ in}} + \dot{m}_c h_c - q_{\substack{rad \\ out}} - (\rho v)_w h_w - \sum_{\ell} \dot{m}_{r_\ell} h_\ell - q_{cond} = 0 \tag{25}$$

where

$$(\rho v)_w = \dot{m}_c - \sum_{\ell} \dot{m}_{r_\ell} \tag{26}$$

The relation $q_{cond} = f(T_w)$ is delivered by the in-depth solution. Other dependencies of interest are

$$h_c = h_c(T_w) \tag{27}$$

$$q_{\substack{rad \\ out}} = q_{\substack{rad \\ out}}(T_w) \tag{28}$$

For the other terms, we may write in general

$$T_w,\ -q_a,\ q_{\substack{rad \\ in}},\ h_w,\ \sum_{\ell} \dot{m}_{r_\ell} h_\ell = \begin{array}{l}\text{functions of boundary-layer-edge enthalpy, pressure, local boundary-layer solution, laws for conservation of chemical elements, chemical equilibria and/or kinetic relations, upstream events, } \dot{m}_c\end{array} \tag{29}$$

If the boundary layer transport aspects of the problem are modeled by a film coefficient scheme, then Equation (25) can be normalized on the mass transfer coefficient in the customary manner:

$$\frac{-q_a}{\rho_e u_e C_M} + \frac{q_{\substack{rad \\ in}} - q_{\substack{rad \\ out}}}{\rho_e u_e C_M} + B'_c h_c - B' h_w - \sum_{\ell} \frac{\dot{m}_{r_\ell}}{\rho_e u_e C_M} h_\ell - \frac{q_{cond}}{\rho_e u_e C_M} = 0 \tag{30}$$

and relationship (29) becomes

$$T_w, \frac{-q_a}{\rho_e u_e C_M}, \frac{q_{rad\ in}}{\rho_e u_e C_M}, h_w, \sum_{\ell} \frac{\dot{m}_{r_\ell}}{\rho_e u_e C_M} h_\ell = \text{functions of boundary layer edge enthalpy, pressure, laws for conservation of chemical elements, chemical equilibrium and/or kinetic relations, } B'_c \tag{31}$$

The generation of these relationships is the goal of Phase IV, the surface thermochemistry solution, to be discussed below. For the present, it may be observed that the energy balance coupling proceeds as follows: an initial guess of the dimensionless mass removal rate B'_c is obtained in some manner. With this B'_c, the quantities $-q_a/\rho_e u_e C_M$, h_w, $\sum \dot{m}_{r_\ell} h_\ell / \rho_e u_e C_M$, and T_w are obtained from the surface thermochemistry solution. The quantities h_c and $q_{rad\ out}$ are then formulated using the T_w so obtained. The surface energy balance is then computed, the q_{cond} as a function of T_w having been provided by the in-depth solution. In general, however, the sum of the terms will not equal zero, but some error. An iteration procedure is then used to select successively better estimates of B'_c which drive the error to zero. Experience shows that Newton's procedure, in which the derivative of the error with respect to B'_c is used to compute the next guess for B'_c gives good results.

4.2 COMPUTATIONAL APPROACHES

4.2.1 Pre-calculated Table

It is evident that each iteration in the search for a surface energy balance, if performed as described above, would require a new surface chemistry solution, generally in the near neighborhood of many such previous solutions. If this state solution is to be obtained from a large subprogram (rather from, say, simple correlations), this constant repetition of thermochemistry calculations would consume an unacceptable amount of computer time. This suggests that a tabular approach in which the surface state solutions are done beforehand for preassigned B'_c values would offer significant computational economies. As an example of this approach, consider one body point. Assume, for simplicity, that chemical kinetics are not important; then the independent variables in Equation (31) reduce to pressure P, boundary layer recovery enthalpy H_r, and B'_c. Figure 13 represents the space of these three independent variables. The course of a typical transient solution might be as represented

in the sketch. As time proceeds, solutions progress

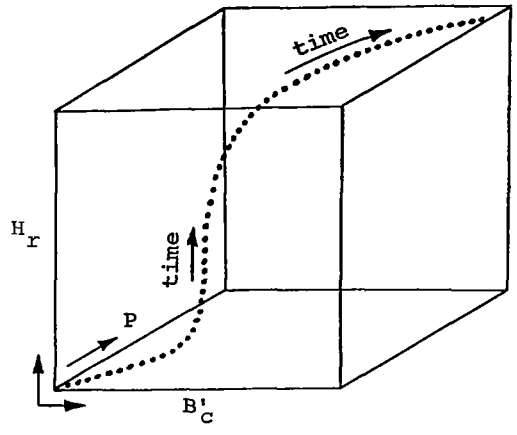

Figure 13. Representation of Course of Independent Variables in Surface History, One Body Point

through the space of the table independent variables B'_c, H_r, and P. The dots in the picture represent solutions satisfying the surface energy balance as time progresses. Surrounding these points are a number of other points examined during the iterations to satisfy the surface energy balance. For any iteration, the solution procedure finds itself, so to speak, within a cube formed by the bracketing tabular values of B'_c, H_r, and P. The dependent quantities T_w, $-q_a/\rho_e u_e C_M$, h_w and $\sum \dot{m}_{r_\ell} h_\ell / \rho_e u_e C_M$ have been precalculated for these tabular points; relevant values of these quantities for the current iteration values of B'_c, H_r, and P can then be formed by interpolation inside the cube and the surface energy balance equation calculated. If the energy balance is not satisfied to some preselected degree of accuracy, a new value of B'_c can be selected and the process repeated.

The interpolation feature of the tabular approach drastically reduces the number of surface state calculations while at the same time allowing sufficient accuracy.* The precalculated table approach has the following advantages:

1. In parametric studies, tables once generated are useable for many different problems, yielding even greater economy.

*For example, a typical 2000 time step problem with the usual 5 iterations per time step would require 10,000 surface state calculations, which require 1 to 3 seconds each for machines in the 7094 speed class. A single enthalpy table, on the other hand, might involve only about 300 state solutions (30 B'_c values times 10 pressures), a factor of 30 improvement. Multiple enthalpy tables reduce this advantage, but usually only a few enthalpies are required.

2. For most problems, it is difficult to specify a priori an "adequate" array of independent tabular values B'_c, H_r, and P. An examination of the precalculated surface tables before execution of the actual ablation-problem-plus-in-depth-solution can reveal if there are any "holes" in the tables in areas where energy terms are varying rapidly. Desirable table points can be added before the in-depth response run.

3. The surface tables are frequently of independent interest in themselves for judging the ablation effects under various conditions.

4. Finally, without the tabular approach, the occasional nonconvergent surface chemistry solution would stop the entire in-depth solution process. With the precalculated table approach, such solutions are automatically weeded out of the tables without damage to the subsequent in-depth solutions.

On the other side of the ledger, some big disadvantages in the precalculated table approach are evident however:

1. Figure 13, which is a realistic schematic view of a typical calculation history, indicates that most of the laboriously calculated and assembled surface state points in the table are never used in the course of a given solution.

2. The "mechanical" linkage between the surface state solution and the in-depth solution, i.e., the transfer of punched card surface state output to input of the in-depth program, leads to computing delays and occasionally to gross input blunders (wrong decks, missing parts of decks, etc.).

3. Too much storage is required by the large precalculated table.

4. The system cannot readily be generalized to accomodate more parameters. Both storage requirements and computation time grow out of reasonable bounds.

This last difficulty would prove to be a great stumbling block in the ablation code described here, which considers chemical kinetics in addition to the other independent variables B'_c, H_r, and P described above. "Kinetics" contribute a fourth parameter in the following manner: The chemical state routine considers a number of simultaneous equations including element balances, equilibrium relations, and kinetically controlled reactions (References 4 and 5). Each kinetically controlled reaction equation has one forward rate coefficient, which in turn comprises one pre-exponential factor B'_m (for the m^{th} such reaction) and a temperature dependent quantity. All

equations are normalized on the transfer coefficient $\rho_e u_e C_M$; this yields the desired independent variable B' in the element balances and also produces normalized kinetic rate coefficients $B_m/\rho_e u_e C_M$. Thus any forward rate coefficients used in the state routine are input in the form $B_m/\rho_e u_e C_M$, and the whole set of $B_m/\rho_e u_e C_M$ values characterizes the role of kinetics. In a given problem the set of B_m's is fixed; thus really there is only one parameter scaling the kinetic effects. Exactly what this parameter is called is not important; let it be termed $B_1/\rho_e u_e C_M$ where B_1 represents the first of the set of kinetically controlled reactions considered.

Thus the four problem variables, which would be the independent variables in the prepared table, are:

1. Ablation rate B'_c
2. Kinetics parameter $B_1/\rho_e u_e C_M$
3. Recovery enthalpy
4. Pressure

Four independent variables are plainly very troublesome. First, the savings in computation time are seriously compromised, since the number of preprepared solutions has gone up by a large number. Second, machine storage requirements are now inconvenient; several dependent variables must be stored at each point in an array which might include 30 x 10 x 10 x 10 = 30000 points. These difficulties in the pre-calculated table approach lead to the invention of a revised tabular approach described in the next sub-section.

4.2.2 Direct-Coupled Table

4.2.2.1 General Description

It is obvious that the difficulties involved in the precalculated table approach to a "four-dimensional table problem" could be removed with a "close-coupling" procedure which only called for calculation of tabular values as they are needed during the actual in-depth solution*. At any instant, the surface-energy-balance-plus-in-depth response solution procedure first examines the corners of the "square" (or "cube", depending on the number of independent variables) it finds itself in, to see if the necessary dependent quantities have been computed and stored. If not, the in-depth routine returns to a master control routine and asks that any missing values be supplied. The master control routine determines which corners

*Another way out, not considered here, is to reduce the number of parameters from four to two by ignoring kinetics and by assuming equal diffusion coefficients and $C_M = C_H$. For this "classical" simple case, as is well known, the edge state does not enter the determination of the surface state, and one can use the same two parameter surface table in which B'_c and P are the independent quantities, for all surface locations and all times.

need filling, calls the surface state program to fill them, and then returns to the in-depth routine, which continues with the problem solution.

Such an approach minimizes the number of state points calculated, since the four parameters in the list above shrink to only three because the second, third, and fourth variables ($B_1/\rho_e u_e C_M$ and edge state) can now be directly associated with time as the solution progresses, although when this is done axial stations must be distinguished from each other, since each station will have different time histories. There is a net decrease of one in the number of independent variables. If the tables were to be pre-calculated, the three variables would, of course, require separate arrays specified in advance, since the true histories of $\rho_e u_e C_M$ and edge state are consequences of the solution due to body shape effects. With direct coupling, $B_1/\rho_e u_e C_M$ and the edge state are effectively known functions of time for each station since the body shape is to be calculated at each instant. Thus the independent variable list becomes:

1. Ablation rate B'_c
2. Axial station
3. Time

Thus the direct coupled approach brings us back to a three-parameter system and the same general economics as before. Another computational economy is introduced since in general this array will not be completely filled in the course of a transient problem.

Additional economies of computer storage are realized since only two table values of time are involved in the calculation at any one instant. Instead of having to store a whole box of solutions of the sort shown in Figure 13, the program needs to store at any one time only adjacent "sheets" of one box as indicated in Figure 14. As soon as the time passes out of the interval between the two sheets, the earlier (θ_n) of these two sheets is discarded and a new sheet at θ_{n+2} (temporarily empty of any dependent solution values) added.

Thus the direct coupled approach puts the "more-than-three-parameter-table" problem within reach economically speaking, and renders it more

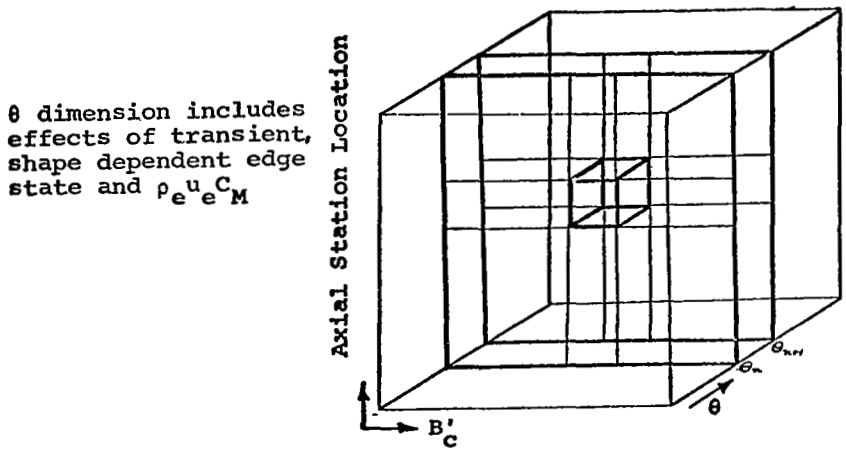

Figure 14. Sketch Indicating Solution Space and Solution "Sheets" Stored at Any Instant During Solution

economical than the precalculated three-parameter table approach. Furthermore, it reduces computer storage considerably and reduces mechanical handling problems of punched tables.

However, in this direct-coupled scheme two important procedural matters have to be considered. These will be described in the following sub-section.

4.2.2.2 Some Dangers in the Direct-Coupled Table Approach

The general attractiveness of the direct-coupled table approach is somewhat compromised by two potential problems:

1. The user will probably want to specify in advance the array of tabular independent B'_c values. But what if he makes a poor choice, so that the in-depth solution has trouble finding a surface-energy balance with the tabular values provided? Can a scheme be devised to rescue the problem solution by automatically inserting new tabular B'_c values in unforeseen critical or difficult areas of the table?

2. What can be done about the occasional nonconvergent surface state solution obtained from the surface state program? Experience shows that it is not possible to guarantee a converged solution from complex surface chemistry routines; in any surface table array usually some of the points prove to be unobtainable without some human intervention in the form of better first guesses for the surface state program. In the coupled program, the in-depth scheme must be able to adjust to this fact and continue calculating

even in the occasional absence of a converged entry in the surface state table.

The code described here does not contain an automatic answer to the first problem. A somewhat similar coupled code (Reference 6) used for charring materials of very complex composition has shown that such a feature is less necessary than might be supposed a priori. In any event, a generally worthwhile scheme would be very difficult to devise. The code does contain, however, a very valuable feature which successfully meets most of the difficulties which arise under point number 1. above. Carbon ablation in air provides a worthwhile example. Figure 15 shows the dependence on temperature of carbon ablation rates in air. Over a wide range of temperature B_c' is for all practical purposes independent of temperature; in this range the only useful independent variable in the surface thermochemical solution process is temperature, since it would be nearly impossible to select a sequence of B_c' values distributed along the plateau.

Therefore, the description presented above, in which B_c' was used as one of the independent variables, should be extended to include temperature as an independent variable in place of B_c', at least in some cases. Figure 15 also shows, however, that temperature is not a good independent variable in some instances.

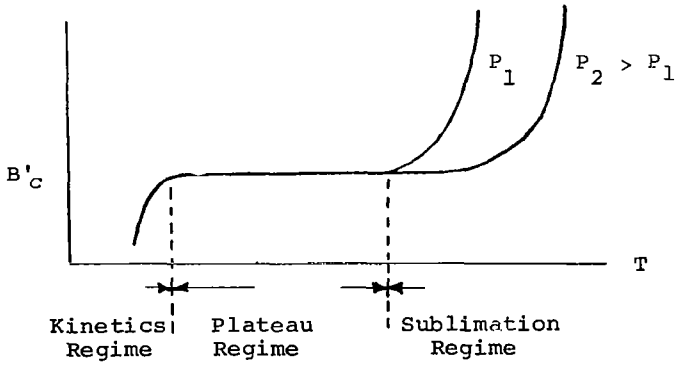

Figure 15. Ablation Rate B_c' Versus Temperature for Carbon in Air

At high temperatures B_c' becomes strongly dependent on T, so that B_c' is the preferred independent variable.

This general problem is rather typical, it turns out. Consequently the single independent variable represented by B_c' in Figure 14 has, in the code, a more complex dual nature. The variable begins with a string of ascending surface temperature (not B_c') values (chosen by the user) and concludes with a string of ascending B_c' values (also chosen by the user).

During the solution process, the MACABRE code calls for surface state solutions at the minimum (first) B'_c value in each B'_c string and notes the temperature discovered for this point. Temperature points in the temperature string above this temperature are ignored. In solving for the surface energy balance at a given point at a given time, the code compares the previously formed surface temperature T_w to the two temperatures at the first B'_c values for each of the two time sheets currently stored. If T_w is less than either of these two values, the surface energy balance iteration process will refer only to the user-assigned temperature part of the table (with B'_c's and other dependent information at each tabular point discovered as necessary by calls to the chemistry routines). Otherwise, the iteration process will refer to the user-assigned B' part of the table (with T_w's and other dependent information discovered in a similar manner as needed).

This dual nature mechanism solves many of the difficulties which might otherwise arise under point 1. above. The user must still exercise some caution, however. For example, in the case illustrated by Figure 15, the code user might begin his sequence of independent variables with temperature entries starting at the lowest temperature of interest (say, 530°R) and extending up to (as a minimum objective) the point where B'_c begins to rise above the plateau value for the lowest pressure to be encountered. It would be conservative and preferable to add temperatures even beyond the "rise point" at the highest pressure in case these points should be needed during the solution.

After these temperature values, B'_c's may be added to span the expected range of B'_c's. The user must be careful to pick a minimum B'_c slightly above the plateau value. A B'_c value near the start of the plateau or off the plateau in the low temperature region is extremely undesirable for two reasons:

1. The lowest assigned B'_c determines the break between assigned temperature solutions and assigned B'_c solutions; a low B'_c will in effect "disqualify" all of the assigned temperature points across the plateau and leave a large "hole" in the array of surface thermochemical solutions.

2. For equilibrium calculations, assigned B'_c solutions at B'_c values below the plateau have a high probability of non-convergence difficulties in the chemistry routines.

The second practical difficulty cited above for the direct coupled table approach concerns possible non-convergent solutions in the chemistry routines. Strictly speaking, even one such solution should serve to halt the entire solution process, but fortunately the situation usually does not demand such drastic action. The chemistry routines allow a certain number of iterations to find the state solution; failure to converge within the pre-

set allowed number of iterations is rare and usually means that the solution either is oscillating in the very near neighborhood of the true solution or has arrived near to the solution and is proceeding very slowly toward it. Therefore, usually the MACABRE code may safely accept a certain number of non-converged answers. Beyond this limit, the computation is stopped as a safety measure, since repeated failures to converge are usually due to large input blunders.

4.2.2.3 The Other Independent Variables in the Direct Coupled Table

Sub-section 4.2.2.2 above has described in some detail the user input of the T_w/B'_c string of independent variable values. There are, of course, two additional independent variables, but fortunately these are quite simple.

The first of these is simply body station or surface point. These are kept separate, each point having its own string of T_w/B'_c values. Thus the histories of all the surface points would appear in Figure 14 as a number of strings of solution points, each wandering in its own horizontal plane (the time $-B'_c$ plane).

The last dimension to be considered, the time dimension, is represented by a user selected string of time values. The same array will be used for all stations. It is not difficult for the user to select a set of values appropriate to the transient nature of a given problem.

Thus, in evaluating the surface energy balance at any given time, the surface energy balance routine refers to stored tabular values of T_w and enthalpy quantities at the two tabular values of time surrounding the current time. If the requisite information has not yet been calculated and stored, the FILL routine calls the thermochemical state program to supply this information. If a "previous time" point (at θ_n in the nomenclature of Section 4.2.2.1 and Figure 14) is being filled in, the thermochemical state is naturally evaluated at stored values of the local independent variables in the chemistry solution, pressure and recovery enthalpy,* at that previous time. If a "future time" table point is being filled in, the FILL routine is obliged to obtain the state solution at future local values of pressure and recovery enthalpy. If the user is not supplying these values as functions of time (and thereby suppressing some of the automatic coupling features of the code; see Section 7 below), then these future values must be estimated. Future local pressure is estimated as the future stagnation pressure times the past ratio of local pressure to stagnation pressure (i.e., based on the correct future stagnation pressure, but the past body shape). Similarly, future local recovery enthalpy is estimated as the future stagnation enthalpy times the ratio of the past local recovery enthalpy to the past stagnation enthalpy.

*The transfer coefficient $\rho_e u_e C_M$ is also an independent variable, as discussed above; if kinetics are being considered it is handled differently, as will be explained below.

(This approximation refers only to "future time" communication with the state routine, for which an approximate future value of H_r is quite adequate since H_r has only a slight effect on the surface thermochemical state evaluation; in the surface energy balance equation evaluation itself, the "properly" computed current recovery enthalpy is used.)

4.2.3 Summary

Three procedures have been considered for coupling a surface state solution to the two-dimensional in-depth solution: direct calculation at every iteration, precalculated tables, and direct coupled tables filled in as the solution progresses. The third was shown to be the only reasonable procedure for a two-dimensional in-depth solution. A suitable coupling procedure requires a logic routine to determine which table points need filling during the surface energy solution process, plus some means of specifying the values of the table independent variables. In the code, the user specifies a priori the sequence of B' values be considered appropriate for each body station, plus a series of time points at which solutions are to be performed.

4.3 THE CONVECTIVE SURFACE ENERGY BALANCE EQUATION

Up to this point, we have been able to discuss the IV-V link between the in-depth solution and the surface thermochemical state solution, which is effected through the convective surface energy balance operation, without discussing the surface energy equation itself except in its general nature, given by Equations (23), (24), (25), (30), and (31). It is now appropriate to consider this equation in more detail. As noted previously, the surface linkages are built upon a transfer coefficient approach: transfer coefficient equations are used for mass diffusion in the element balance equations and a transfer coefficient type of surface energy balance equation is employed in the IV-V linkage.

The proper choice of energy equation constitutes a subject far too large and difficult to discuss completely in this report. The MACABRE code uses one of three different forms of the convective energy equation, depending on user choice. In ascending order of complexity, and descending order of "well foundedness", these equations are

(1) For equal mass diffusion coefficients for boundary layer molecules and for $C_M = C_H$ (Le = 1):

$$H_r - (1+B')h_w + B'_c h_c + \frac{\alpha_w q_{rad\ in}}{\rho_e u_e C_H} - \frac{F\sigma\varepsilon}{\rho_e u_e C_H} T_w^4 = \frac{q_{cond}}{\rho_e u_e C_H} \qquad (32)$$

This equation is a "standard" (see, for example, Reference 7) one and requires no discussion.

(2) For equal diffusion but $C_M \neq C_H$ (Le $\neq$ 1):

$$(H_r - h_w)_{\substack{\text{edge}\\\text{gas}}} + \frac{C_M}{C_H}\left[\sum_i (K_{i_e} - K_{i_w})h_i^{T_w} + B_c'h_c - B'h_w\right]$$

$$+ \frac{\alpha_w q_{\text{rad in}}}{\rho_e u_e C_H} - \frac{F\sigma\varepsilon T_w^4}{\rho_e u_e C_H} - \frac{q_{\text{cond}}}{\rho_e u_e C_H} = 0 \qquad (33)$$

This equation supposedly accounts for $C_M \neq C_H$ effects, and doubtless does so if the boundary layer is frozen. The accuracy of Equation (33) for chemically active boundary layers has been much discussed and the question remains open (References 7, 8, 9).

(3) For unequal diffusion:

$$(H_r - h_w)_{\substack{\text{edge}\\\text{gas}}} + \frac{C_M}{C_H}\left[\sum_i (Z^*_{i_e} - Z^*_{i_w})h_i^{T_w} + B_c'h_c - B'h_w\right]$$

$$+ \frac{\alpha_w q_{\text{rad}}}{\rho_e u_e C_H} - \frac{F\sigma\varepsilon T_w^4}{\rho_e u_e C_H} - \frac{q_{\text{cond}}}{\rho_e u_e C_H} = 0 \qquad (34)$$

This equation, introduced in Reference 10, appears to be useful for modeling unequal diffusion effects, at least in frozen boundary layers, and currently is being studied in detail to establish its validity (Reference 9).

All three of these equations (32), (33), and (34) serve to provide expressions for the diffusion energy flux $-q_a$ in Equation (30). The constituents of $-q_a$, which include $h_{w_{\substack{\text{edge}\\\text{gas}}}}$, $\Sigma Z^*_{i_e} h_i^{T_w}$, and $\Sigma Z^*_{i_w} h_i^{T_w}$ are generated by the chemistry routines along with h_w and T_w. The subroutine FILL, which calls the chemistry routines, then combines the quantities in the appropriate fashion as dictated by Equation (34) or one of the simpler forms (33) and (32). For example, suppose the FILL routine discovers a requirement for a state solution at a tabular B_c' and for a given pressure and recovery enthalpy. FILL calls the state routines, controlled by EQUIL, which perform the state solution, evaluate key property values, and return to FILL values T_w, h_{w_e}, $\Sigma Z^*_{i_e} h_i^{T_w}$, h_w, $\Sigma Z^*_{i_w} h_i^{T_w}$. FILL then, referring

to the temperature T_w, looks up the ablating material enthalpy h_c and constructs the term

$$Y = -h_{\substack{w_{edge} \\ gas}} + \frac{C_M}{C_H}\left[\sum(Z^*_{i_e} - Z^*_{i_w})h_i^{T_w} + B'_c h_c - B' h_w\right]$$

and stores it as one of the dependent quantities of interest. The temperature T_w is stored as the second dependent quantity of interest. (On the assigned T_w lower part of the table, EQUIL returns B'_c and this is stored.)

4.4 CONVECTIVE SURFACE ENERGY BALANCE ITERATION PROCEDURE

At every surface point at which a convective energy balance is to be obtained, the energy balance subroutine must

(a) decide whether T_w or B' is the proper independent variable to iterate

(b) select a trial value of this independent variable

(c) refer to stored dependent values of energy quantity Y and temperature T_w (or B'_c if in first part of table), interpolating as necessary on B'_c and θ, and filling in needed table points as necessary by calling FILL

(d) look up $\alpha_w(T_w)$ and $\varepsilon_w(T_w)$, $q_{\substack{rad \\ in}}(\theta)$, local F, plus C_M, C_H, and $H_r(\theta)$ (which in many cases are generated by special subroutines described in Sections 8 and 9 below)

(e) formulate the left-hand side of Equation (34), note departure from zero (error ε)

(f) if error is too large, correct trial value of independent variable, go to (c).

Generally this process converges very fast, usually within three of four iterations. Step (f), the correction step, is based upon the Newton-Raphson procedure: at the same time the error ε is being computed, the derivative of the error with respect to the independent variable is also formed, using derivatives of the tabular quantities Y and T_w (or B'_c). The correction in the independent variable is then computed directly:

$$\Delta B'_c = -\varepsilon/(d\varepsilon/dB'_c) \tag{35}$$

or

$$\Delta T_w = -\varepsilon/(d\varepsilon/dT_w) \tag{36}$$

4.5 AVOIDING THE SURFACE STATE SOLUTION

The convective boundary condition described so far in this section does not include all problems of interest. Consequently the surface boundary condition treatment has been formulated as a triple option. The first of these (called Option 1) constitutes the convective boundary condition described in Section 4.1-4.4 above. A second option (Option 2) merely refers to input time-dependent quantities for user assigned values of surface temperature and recession rate. A third option (Option 3) retains the energy balance aspects of Option 1, but eliminates the convective heating terms and does not allow surface recession. This option is useful for "cool-down" or "soak -out" portions of problems, and can also be used for assigned heat flux problems in general (through the $q_{rad\ in}$ variable) if surface recession is negligible. The heating option may be changed at the user's choice at any time for a given column or surface station, and the heating option assignments may vary in any manner around the body at a given time.

SECTION 5

SURFACE STATE CALCULATION - PHASE IV

5.1 INTRODUCTION

Section 4 above has described the convective surface energy balance boundary condition and described the use made in this boundary condition calculation of computer subroutines for evaluating various heated surface thermochemical state variables, chiefly enthalpy and molecular composition. For a restricted range of problems it would be possible to avoid the use of chemistry routines for this calculation and instead rely on enthalpy correlations and the like, but for the present coupled code it was strongly desired to have a general ablation program which could treat any non-charring ablating material exposed to any arbitrary environment. Fortunately, suitable thermochemistry routines already existed which could be coupled to the in-depth response code; the program reported here did not develop these chemistry codes. Since these codes are fully described elsewhere (References 4 and 5) this section will seek only to give a general overview of the physical problems treated by the chemistry routines.

The thermochemical routines as a package are referred to as ACE, after Aerotherm Chemical Equilibrium code. This is an inappropriate acronym since (1) the routines consider non-equilibrium chemistry as well as equilibrium, and (2) in the coupled code no routine has the name ACE; the controlling routine is called EQUIL. For historical reasons, however, we shall continue to call the thermochemistry package ACE.

5.2 USES OF ACE IN MACABRE

The ACE package is called upon for a number of computational tasks in the coupled code. Its main use, of course, is in generating surface thermochemical state solutions. As will be discussed below, these are open system calculations involving interactions between edge gas and the main ablating material. The surface energy equations (33) and (34) include terms like $h_{w_{edge\ gas}}$ and $\Sigma K_{i_e} h_i^{T_w}$ or $\Sigma Z^*_{i_e} h_i^{T_w}$, however, which indicates another needed thermochemical calculation: the molecular make-up of the boundary layer edge gas must be identified and certain properties evaluated (such as $Z^*_{i_e}$). Each call to ACE for a surface state solution in fact involves the following computations:

(1) a closed system equilibrium calculation on edge gas alone to determine K_{i_e} and $Z^*_{i_e}$; this calculation is done at assigned pressure and recovery enthalpy*.

(2) an open system ablation calculation at assigned pressure, $\rho_e u_e C_M$ (for kinetic effects), and either B'_c or T_w (depending on location in independent variable array); this calculation may include kinetic effects

(3) a frozen evaluation of $h_{w_{\substack{\text{edge}\\\text{gas}}}}$ and $\Sigma Z^*_{i_e} h_i^{T_w}$ at temperature T_w.

The quantities $h_{w_{\substack{\text{edge}\\\text{gas}}}}$, $\Sigma Z^*_{i_e} h_i^{T_w}$, h_w, and $\Sigma Z^*_{i_w} h_i^{T_w}$ are obtained from ACE and employed as described in Sections 4.3 and 4.4 above.

(The ACE routine may also be used by the pressure distribution and transfer coefficient routines to generate certain thermodynamic properties and transport properties of the boundary layer gas. These properties are stored for future use in a Mollier Chart (as will be described in more detail in Sections 8 and 9 below) in which P and h_e are the independent variables; the required ACE calculations are therefore closed system equilibrium calculations of the edge gas at assigned pressure and enthalpy.)

The following sections describe the manner in which calculations are done in the ACE package.

5.3 PHYSICAL PROBLEMS TREATED BY THE ACE PACKAGE

The ACE package of subroutines treats a wide range of thermochemical problems. Since these problems are complex, the capabilities of the ACE package can perhaps best be illustrated by a set of descriptions of increasing generality. The following sections describe such a graded series of problems.

5.3.1 Closed System in Equilibrium

Closed systems are defined as those for which the relative amounts of chemical elements are prespecified. The edge gas state calculations are of this type.

Consider K chemical elements, N_k, introduced into a previously

*Good arguments can be made for using the static enthalpy instead, but this proves inconvenient in the code. The difference in results is small in any case.

evacuated container. In general, these elements will interact to form a number of chemical species*, N_i (gas phase) and N_ℓ (condensed phases). If enough time has elapsed so that thermodynamic and chemical equilibrium is established, the thermodynamic state of the system, including the relative amounts of chemical species present, is completely determined if two independent thermodynamic variables are known**. This condition may be stated mathematically by examining the governing equations for such a system, and showing that the number of independent equations is equal to the number of unknown quantities.

Relations expressing the formation of the gaseous chemical species from the gaseous chemical elements may be written as follows:

$$\sum_{K=1}^{K} C_{ki}\, N_k \rightarrow N_i \tag{37}$$

Similarly, formation of condensed phase species from the gaseous elements is written:

$$\sum_{K=1}^{K} C_{k\ell}\, N_k \rightarrow N_\ell \tag{38}$$

In the above, C_{ki} represents the number of atoms of element k in a molecule of species i (gas) or species ℓ (condensed).

If the gas phase species are assumed to individually behave as thermally perfect gases, then the equilibrium relation corresponding to reaction (37) is

$$\frac{P_i}{\prod_{k=1}^{K} P_k^{C_{ki}}} = K_{pi}(T)$$

$$\ln P_i - \sum_{k=1}^{K} C_{ki} \ln P_k = \ln K_{pi}(T) \tag{39}$$

where P_k denotes partial pressure and $K_{pi}(T)$ is the equilibrium constant for the formation reaction (37) of species N_i. For each candidate condensed

*"Chemical species" as used here includes molecular, atomic, ionic, and electron species.

** Duhem's Theorem.

phase species

$$-\sum_{k=1}^{K} C_{k\ell} \ln P_k \lesseqgtr \ln K_{p\ell}(T) \tag{40}$$

where

= indicates the existence of the condensed phase species N_ℓ in equilibrium with gas phase species, and

< indicates that the condensed phase species N_ℓ will not be present in equilibrium.

For each chemical element introduced into the system, the conservation of atoms dictates that the amount of any element k in the gas and condensed phases (regardless of molecular configuration) must sum to the total amount of element k in the system. Mathematically, this may be written, for each element k, as

$$\begin{pmatrix}\text{Mass fraction}\\ \text{of element k}\\ \text{input to the}\\ \text{system}\end{pmatrix} = \frac{\mathcal{M}_k}{\mathcal{M}P}\sum_{i=1}^{I} C_{ki}P_i + \frac{\mathcal{M}_k}{\mathcal{M}}\sum_{\ell=1}^{L} C_{k\ell}X_\ell \tag{41}$$

where $\mathcal{M}$ is a composite system molecular weight* defined by

$$\mathcal{M} = \sum_{i=1}^{I}\frac{P_i}{P}\mathcal{M}_i + \sum_{\ell=1}^{L} X_\ell \mathcal{M}_\ell \qquad \left(\text{units of } \frac{\text{grams of system}}{\text{moles of gas}}\right) \tag{42}$$

and where X_ℓ is a mole fraction of condensed phase species ℓ defined as

$$X_\ell = \frac{\text{molecules of condensed species } \ell}{\text{total gas phase molecules i}} \tag{43}$$

*This is the molecular weight appropriate to the ideal gas equation of state if condensed phases are present.

In addition, for the gas phase species, there exists the requirement that the partial pressures must sum to the total system pressure

$$\sum_{i=1}^{I} P_i = P \tag{44}$$

Mixture thermodynamic properties, such as specific enthalpy, are related to the species concentrations by equations of the form

$$h = \frac{1}{\mathcal{M}P} \sum_{i=1}^{I} P_i h_i + \frac{1}{\mathcal{M}} \sum_{\ell=1}^{L} X_\ell H_\ell \tag{45}$$

Consider now the number of independent equations for the system. The number of gas phase equilibrium relations (39) is equal to the number of gas phase species I minus the number of elements K (because Equations (39) are trivial when i=k). In addition, there exists a relation such as (40) for each of the L candidate condensed phase species in the system. Note that the system temperature is contained implicitly in Equations (39) and (40) through the temperature dependence of the equilibrium constants. There are K conservation of elements Equations (41), one for each atomic element introduced into the system. The requirement that the partial pressures sum to the system pressure (44) contributes one additional equation. For any additional thermodynamic properties of the mixture (enthalpy, entropy, etc.), there exists equations such as (45).

Consider next the variables appropriate to this formulation of the problem. The relative concentrations of the I species in the gas phase are given by the P_i's and the amounts of the L candidate condensed phase species are given by X_ℓ (most or all of which may be zero). In this formulation, the composite system molecular weight, $\mathcal{M}$ is also a variable. There are one each of the mixture thermodynamic variables T, P, h, s, etc. The number of variables and available independent equations may be summarized as

VARIABLES	NO. OF SUCH VARIABLES	EQUATION NUMBER	NO. OF SUCH EQUATIONS
P_i	I	(39)	I - K
X_ℓ	L	(40)	L
$\mathcal{m}$	1	(41)	K
P	1	(44)	1
T	1		
h,s,ρ,...	n	of the type (45)	n
total variables	I+L+n+3	total equations	I+L+n+1

Thus, there are two less equations than there are variables, and so if two independent variables are specified (e.g., P and T) in addition to the elemental composition, then closure is obtained and the chemical and thermodynamic state of the system may, in principal, be determined.

The ACE program performs this determination. That is, to determine the equilibrium thermodynamic and chemical state of any closed system, one needs only to furnish the ACE program with the elemental composition, the candidate gaseous and condensed phase species,* and two thermodynamic properties. One of these properties must be pressure, and the other may be either temperature, enthalpy, or entropy. Given this information, the ACE program will calculate and output the mole fractions of each candidate species, the temperature, enthalpy, entropy, density, effective molecular weight, equilibrium and frozen specific heats, the isentropic exponent, and a few other quantities of potential interest.

As already noted, MACABRE only calls upon ACE for assigned pressure and enthalpy solutions. The edge state is saved momentarily while the open system calculation is performed.

*The ACE program must be supplied certain basic thermodynamic data (described in References 2 and 5) for each candidate species to be considered in a given system. This data is contained in a three card set, one set for each species. A certain amount of judgement is required on the part of the user relative to which candidate species should be included in a given system. Frequently this judgement is avoided by simply inputting data for all species containing combinations of the input elements.

5.3.2 Open Systems in Equilibrium - Simplified Case

The basic theory underlying the treatment of open systems may best be illustrated by examining the equations expressing the conservation of chemical elements and energy at the ablating surface. If the boundary layer is characterized by equal diffusion coefficients, and if no material is removed from the surface in a condensed phase (i.e., no mechanical erosion or liquid layer removal), then these equations take on a particularly simple form for equilibrium systems. This simplified situation will be considered in this section and these considerations will be extended to more generalized cases in Sections 5.3.3 to 5.3.5.

Consider first the fluxes of chemical elements (k) entering and leaving a control surface affixed to the ablating surface. The solid material may be visualized as moving into this surface at a rate $\dot{s}$. If it is assumed that no material is being removed in a condensed phase, then the surface and the fluxes of the k^{th} chemical element may be illustrated as

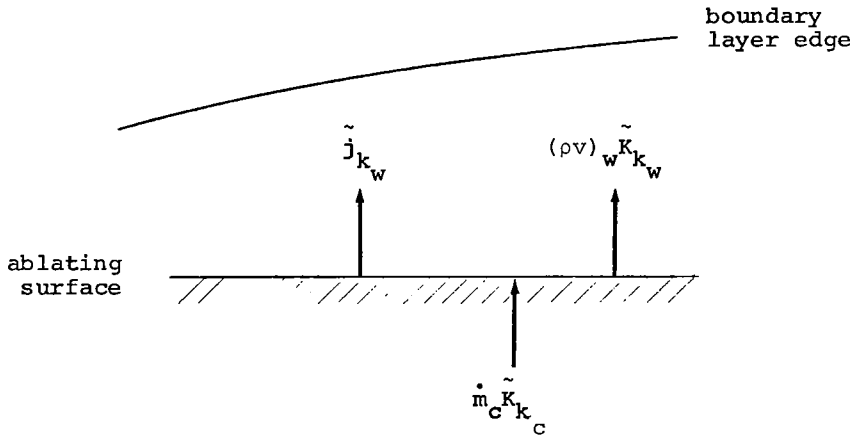

Figure 16. Ablating Surface Mass Balance

Terms superscripted by a tilde (~) represent the total mass fraction or flux of element k, independent of molecular configuration. Thus

$$\tilde{K}_{k_w} = \sum_{i=1}^{I} \alpha_{k_i} K_{i_w} \qquad (46)$$

$$\tilde{j}_{k_w} = \sum_{i=1}^{I} \alpha_{k_i} j_{i_w} \tag{47}$$

where k pertains to element k, i pertains to species i, and α_{k_i} is the mass fraction of element k in species i. Fluxes of element k away from the surface consist of boundary layer diffusion and gross motion of the fluid adjacent to the surface due to the injection flux $\dot{m}_c$.

From the above sketch, it is seen that conservation of chemical elements requires that

$$\tilde{j}_{k_w} + (\rho v)_w \tilde{K}_{k_w} = \dot{m}_c \tilde{K}_{k_c} \tag{48}$$

Summing Equation (48) over all elements k yields the total mass continuity equation (for the case when there is no condensed phase material removal)

$$(\rho v)_W = \dot{m}_c \tag{49}$$

An important fundamental of the present mathematical modeling of the ablation process is the expression of the diffusive heat and mass fluxes in terms of a transfer coefficient formulation.

In this formulation, the diffusional term $-j_{k_w}$ is written

$$-\tilde{j}_{k_w} = \rho_e u_e C_M (\tilde{K}_{k_e} - \tilde{K}_{k_w}) \tag{50}$$

Utilizing this transfer coefficient formulation (50) for the diffusion flux in the elemental balance Equation (48) yields

$$\rho_e u_e C_M (\tilde{K}_{k_w} - \tilde{K}_{k_e}) + (\rho v)_w \tilde{K}_{k_w} = \dot{m}_c \tilde{K}_{k_c} \tag{51}$$

In terms of dimensionless ablation rate B'_c and solving (51) for the total mass fraction of element k at the wall yields (for equal diffusion coefficients and no condensed phase material removal)

$$\tilde{K}_{k_w} = \frac{B'_c \tilde{K}_{k_c} + \tilde{K}_{k_e}}{1 + B'_c} \tag{52}$$

Given the relative amounts of chemical elements specified by (52), the chemical and thermodynamic state of the gases adjacent to the ablating surface may be calculated from equilibrium relations.

Since the gases are in equilibrium with the ablating surface

$$-\sum_{k=1}^{K} C_{k\ell} \ln P_k = \ln K_{p\ell}(T) \tag{53}$$

if ℓ represents the surface species, and

$$-\sum_{k=1}^{K} C_{k\ell} \ln P_k < \ln K_{p\ell}(T) \tag{54}$$

for all other candidate condensed phase species. In the present formulation, (54) may be thought of as being used to identify surface species ℓ for which (53) applies. The equilibrium relations for gas phase species is of the form

$$\ln P_i - \sum_{k=1}^{K} C_{ki} \ln P_k = \ln K_{pi}(T) \tag{55}$$

and the partial pressures must obey the relation

$$\sum_{i=1}^{I} P_i = P \tag{56}$$

The elemental mass fractions adjacent to the surface, $\tilde{K}_{k_w}$, of (52) are related to the species partial pressures, P_i, by relations such as

$$\tilde{K}_{k_w} = \frac{m_k}{P\bar{m}} \sum_{i=1}^{I} C_{ki} P_i \tag{57}$$

Thus, if P is known and B'_c is specified (this may be varied parametrically as will be discussed subsequently), and if T_w and P_i are unknowns, then the number of unknowns and equations available may be summarized as

UNKNOWNS	NO. OF SUCH UNKNOWNS	EQUATION NO.	NO. OF SUCH EQUATIONS AVAILABLE
P_i	I	(55)	I-K
$\tilde{K}_{K_w}$	K	(53)	1
$\dot{m}$	1	(52)	K
T_w	1	(56)	1
		(57)	K
Total Unknowns	I+K+2	Total Equations	I+K+2

Thus, closure is obtained and, in principal, the temperature and chemical composition of the gases adjacent to the surface may be determined if P and B'_c are specified. From the pressure, temperature, and chemical composition, the calculation of other thermodyanmic properties (enthalpy, etc.) is straightforward.

The ACE package of programs has the capability to determine the chemical and thermodynamic state of the gases adjacent to an ablating surface in a fashion similar to that discussed here. In the coupled MACABRE code, the ACE group is typically called with pressure P known and B'_c assigned as an independent variable by the user. The temperature T_w and other state data are then determined. Alternatively, T_w may be assigned (in the lower temperature parts of the tables, as discussed in Section 4.2.2.2 above) and B'_c is determined.

5.3.3 Open Systems in Equilibrium - Unequal Diffusion Coefficients

The discussion of the previous section was limited to open systems with equal species diffusion coefficients and no removal of surface material in the condensed phase. These simplifications were made in order to render the basic theory easier to explain. While this simple model is reasonably accurate for many ablation situations, these assumptions are inappropriate for others. For this reason, calculations performed by the ACE package (and hence the MACABRE program) are not restricted to any of these simplifications. The extension to unequal diffusion coefficients will be discussed first, in this section.

The unequal diffusion coefficient model has already been briefly introduced in Section 4.3 above, in which Equations (33) and (34) may be compared. In simplistic terms, the model replaces the mass fraction during forces K_{i_e} with modified driving forces $Z^*_{i_e}$. A similar modification must be made in the ACE treatment. The diffusive flux of element k at the wall is now modeled by

$$\tilde{j}_{k_w} = \rho_e u_e C_M (\tilde{Z}^*_{k_w} - \tilde{Z}^*_{k_e}) \tag{58}$$

In (58), $\tilde{Z}^*_k$ is, in effect, a weighted average of the mole and mass fractions of element k. The $\tilde{Z}^*_k$ are defined by

$$\tilde{Z}^*_k = \sum_{i=1}^{I} C_{ki} Z^*_i \tag{59}$$

$$Z^*_i = \frac{Z_i^{\gamma} K_i^{1-\gamma}}{\sum_{i=1}^{I} Z_i^{\gamma} K_i^{1-\gamma}} \qquad \text{(where } \gamma \approx 2/3\text{, see Ref. 10)} \tag{60}$$

$$Z_i = \frac{K_i/F_i}{\sum_{i=1}^{I} K_i/F_i} \tag{61}$$

where the F_i are diffusion factors defined by the following relation for the binary diffusion coefficients

$$\mathcal{D}_{ij} = \frac{\bar{D}}{F_i F_j} \tag{62}$$

where $\bar{D}$ is a constant for a given temperature and pressure and the F_i depend weakly on temperature. The $\mathcal{D}_{ij}$ must obey (62) in order for the boundary layer species diffusion equations to reduce to a form from which (58) can be inferred by similarity arguments. Reference 11 demonstrates that the binary diffusion coefficients for a variety of chemical systems are accurately correlated by (62). This reference also shows that a reasonably good correlation equation for the F_i is

$$F_i = \left(\frac{\mathcal{M}_i}{\mathcal{M}_{ref}}\right)^{\varepsilon} \quad \text{where} \quad \mathcal{M}_{ref} \approx 23.4 \quad \text{and} \quad \varepsilon \approx 0.431 \tag{63}$$

when $\bar{D}$ is taken as the self-diffusion coefficient of O_2. Additional discussion relative to this unequal diffusion coefficient formulation is contained in Appendix A.

Consideration of unequal diffusion coefficients affects the surface elemental balance relationships which are needed to determine the equilibrium thermochemical state at the surface. Substituting (58) into (48) yields

$$\rho_e u_e C_M (\tilde{Z}^*_{k_w} - \tilde{Z}^*_{k_e}) + (\rho v)_w \tilde{K}_{k_w} = \dot{m}_g \tilde{K}_{k_g} + \dot{m}_c \tilde{K}_{k_c} \tag{64}$$

and the "unknowns" here are $\tilde{K}_{k_w}$ and $\tilde{Z}^*_{k_w}$, each of which may be expressed in terms of the species partial pressures

$$\tilde{K}_k = \mathcal{M}_k \frac{\sum_{i=1}^{I} C_{ki} P_i}{\sum_{i=1}^{I} \mathcal{M}_i P_i} = \frac{\mathcal{M}_k}{P \mathcal{M}_g} \sum_{i=1}^{I} C_{ki} P_i \tag{65}$$

and

$$\tilde{Z}^*_k = \mathcal{M}_k \frac{\sum_{i=1}^{I} C_{ki} P_i / F_i^{\gamma}}{\sum_{i=1}^{I} \mathcal{M}_i P_i / F_i^{\gamma}} = \frac{\mathcal{M}_k \bar{F}}{P \mathcal{M}_g} \sum_{i=1}^{I} C_{ki} P_i / F_i^{\gamma} \tag{66}$$

where $\mathcal{M}_g$ is the mean molecular weight of the gas phase and $\bar{F}$ is a mean F_i^{γ} defined as

$$\bar{F} \equiv \frac{\sum_{i=1}^{I} \mathcal{M}_i P_i}{\sum_{i=1}^{I} \mathcal{M}_i P_i / F_i^{\gamma}} \tag{67}$$

Substituting these expressions into (64) and utilizing the definition of B'_c, yields an expression for the species partial pressures at the surface in terms of quantities at the boundary layer edge and in the material

$$B' \sum_{i=1}^{I} C_{ki} P_{iw} + \bar{F} \sum_{i=1}^{I} C_{ki} P_{iw} / F_i^{\gamma} = \frac{P \mathcal{M}_g}{\mathcal{M}_k} \left(\tilde{z}^*_{k_e} + B'_c \tilde{K}_{k_c} \right) \tag{68}$$

Note that (68) reduces to (52) when the diffusion coefficients are equal.

When performing unequal diffusion coefficient open system calculations, the ACE program utilizes (68) rather than (52) as the elemental mass balance equations. Other than this, the solution philosophy is essentially as discussed in Section 5.3.2. The diffusion factors utilized in the ACE program may be calculated in three ways, at the user's option

a. diffusion factors F_i may be input individually for each species i

b. diffusion factors may be calculated according to (63) with the user specifying the reference molecular weight, $\mathcal{M}_{ref}$, and the exponent ε

c. if the user does nothing special, the program will calculate F_i according to (63) with $\mathcal{M}_{ref} = 23.4$ and $\varepsilon = 0.431$.

The actual program input for these alternatives is discussed in Reference 2. It should also be pointed out that the diffusion factors have an effect on the other transport properties calculated by the ACE program, and these are briefly discussed in Appendix A.

For unequal diffusion coefficients, the transfer coefficient formulation for the surface energy equation is Equation (34). Consistent with (34), for unequal diffusion coefficient problems, the surface thermochemistry quantities prepared by the ACE program include the quantity

$$\sum_{i=1}^{I} z^*_{i_w} h_i^{T_w}$$

in addition to the quantities previously discussed. Note again, that for

equal diffusion coefficients

$$\sum_{i=1}^{I} Z^*_{i_w} h_i^{T_w} = \sum_{i=1}^{I} K_{i_w} h_i^{T_w} = h_w$$

Similarly, the quantities

$$\sum_{i=1}^{I} Z^*_{i_e} h_i^{T_w}$$

and

$$h_w \quad \begin{matrix}\text{frozen} \\ \text{edge gas}\end{matrix}$$

are computed after reference to the previous automatically computed and stored edge solution.

5.3.4 Open Systems In Equilibrium - With Condensed Phase Surface Material Removal

Considerations to this point have been based on the assumption that all the mass leaving an ablating surface is in the gas phase and this flux has been denoted by $(\rho v)_w$. However, for many ablation situations of interest, some of the material leaving the surface is in a condensed phase - e.g., liquid layer removal or "mechanical ablation". The condensed phase removal affects both the surface mass and energy balances (Reference 10). For the surface elemental balance, there is an additional flux term

$$\sum_{\ell=1}^{L} \dot{m}_\ell \tilde{K}_{k_\ell}$$

leaving the surface. This results in the surface elemental balance (in terms of the species partial pressures - analogous to (68) having the form

$$B' \sum_{i=1}^{I} C_{ki} P_{iw} + \bar{F} \sum_{i=1}^{I} C_{ki} P_{iw} \Big/ F_i^{\gamma} = \frac{P m_g}{m_k} \left(\tilde{Z}^*_{k_e} + B'_c \tilde{K}_{k_c} - \frac{\sum_{\ell=1}^{L} \dot{m}_\ell \tilde{K}_{k_\ell}}{\rho_e u_e C_M} \right) \qquad (69)$$

for each atomic element k. Summing over all elements yields the obvious net mass continuity relation

$$\dot{m}_c = (\rho v)_w + \sum_{\ell=1}^{L} \dot{m}_\ell \tag{70}$$

Similarly, there is an additional energy flux term

$$\sum_{\ell=1}^{L} \dot{m}_\ell H_\ell$$

leaving the surface. The surface energy balance equation becomes (analogous to (34)

$$\rho_e u_e C_H (H_r - h_w)_{\substack{\text{frozen} \\ \text{edge gas}}} + C_M \left[\sum (Z_{i_e}^* - Z_{i_w}^*) h_i^{T_w} + B_c' h_c - \sum \dot{m}_\ell H_\ell - (B')_w H_w \right] + q_{\text{rad in}} - \sigma \varepsilon T_w^4 = q_{\text{cond}} \tag{71}$$

The condensed phase surface material removal model currently incorporated in the ACE program is termed a "fail temperature model". According to this model, a "fail temperature", $T_{\text{fail-}\ell}$, may be pre-assigned to any candidate condensed phase species ℓ. This species will then be removed from the surface (in a condensed phase) at a rate $\dot{m}_\ell$ *if* the surface temperature is greater than, or equal to, the fail temperature for this species. Additional comments relative to the computational aspects will follow a brief discussion of the fail temperature concept.

The fail temperature is the temperature at which the material "fails", i.e., the temperature above which the material will not remain affixed to the surface. For melting solids for which a liquid layer is unstable, the fail temperature is simply the melt temperature. For thermochemically eroding solids, the fail temperature might be set at some temperature characteristic of the material yield temperature at the appropriate external loading. Also, the ACE program has a provision for inputting a maximum fail temperature for all condensed species. Physically, this maximum fail temperature might correspond to the fail temperature of the substrate.

When failing occurs, an additional equilibrium relation is available for each condensed phase species ℓ for which $\dot{m}_\ell > 0$. Also the surface

temperature must be consistent with the assignment fail temperatures:

$$T_w \leq T_{fail} \text{ for the surface species}$$

$$T_w \geq T_{fail} \text{ for any species for which } \dot{m}_\ell > 0$$

These additional equilibrium relations, surface temperature restrictions, and assigned fail temperatures are sufficient to solve for the additional unknowns $\dot{m}_\ell$ introduced into elemental mass balance relations. The enthalpy, H_ℓ, of the condensed phase being removed is determined from the species thermochemical data. If $T_{fail} < T_{melt}$, H_ℓ is taken as the enthalpy of the solid, and if $T_{fail} \geq T_{melt}$, H_ℓ is taken as the enthalpy of the liquid. The convention for associating fail temperatures with each or all candidate condensed phase species will be specified in Reference 2*.

In communicating back to MACABRE, the ACE package amalgamates the terms $(\rho v)_w H_w$ and

$$\sum_{\ell=1}^{L} \dot{m}_\ell H_\ell$$

by suitably modifying the returned value of H_w. Thus FILL constructs the quantity Y as described in Section 4.3 without specific reference to failing events.

5.3.5 Non-Equilibrium Effects in Open System Calculation

To calculate the equilibrium state of a chemical system, information relative to all chemical reactions is not needed. This fact permits a significant simplification in the problem formulation, and those features of the ACE package discussed thus far take advantage of these simplifications. For some systems of interest, however, the effects of reaction kinetics may not be neglected. A general solution of complex problems for which reaction kinetics effects are important is potentially difficult for at least two reasons: a) there are significant computational and bookkeeping problems associated with the analytical treatment of mixed equilibrium and nonequilibrium systems, and b) for many systems of engineering interest, the rate controlling reactions are not well known and/or rate constants for these reactions are unavailable. The ACE package of routines effectively

*For carbon ablation in air, the fail temperature concept is of almost no interest. Graphites loaded with metals, however, tend to form thin oxidation resistant oxide coatings which generally ablate by melting. The ACE package will properly identify any such oxides formed, and the fail temperature mechanism allows them to be ablated realistically. Fail temperatures are useful for metal heat shields, of course.

surmounts the first of these problems as discussed in Reference 4 and as will be briefly summarized subsequently. However, difficulties falling into the second category above frequently preempt any such "exact" analytical treatment. In these cases, various approximate treatments can often yield useful information. These approximate treatments essentially consist of not allowing certain species, or groups of species, to react with an otherwise equilibrated system. A few examples of this sort of approximate treatment will be discussed in the following paragraphs. These discussions will be followed by a brief summary of the general kinetics option of the ACE program.

5.3.5.1 Removal of Selected Species from the System

The simplest, and perhaps the crudest, way to approximate certain kinetic effects is to simply remove from the equilibrium system those species whose formation is, in reality, suppressed by reaction kinetic effects. Computationally, these species are removed merely by removing the thermochemical data cards for that molecule from the species thermochemical data deck. (Reference 2 describes this deck in detail.)

5.3.5.2 Isolated Species

Certain chemical species may be frozen individually at any given concentration. This treatment is sometimes useful for species which are relatively nonreactive because of chemical kinetic effects. For example, consider the flow of a C-O-H gas over a relatively low temperature ablating carbon surface. Isolation of H_2O at its boundary layer edge concentration would provide a more realistic surface thermochemistry table than if full equilibrium were assumed (since the water-gas reaction at the surface is relatively slow at lower temperatures). In the ACE program, this isolation of species is achieved by treating that particular species as an atomic element, an element with a fictitious atomic number so that it cannot react chemically with any other members of the chemical systems. Computationally, this requires specification of the input of the appropriate quantity of this "element" (accompanied by appropriate reductions in the amounts of other actual elements), and the alteration of the species thermochemistry data card set for that species so that it contains only one "atom" of the fictitious "element."

5.3.5.3 Isolated Subgroups of Elements

In some practical applications, there exists a subgroup of elements which are in equilibrium with each other, but the subgroup is not in chemical equilibrium with the system as a whole. The isolation of a subgroup of elements can be achieved by considering these elements to be different "elements" with properties the same as, but with atomic numbers different from, the corresponding actual elements (e.g., add 100 to the atomic numbers of the elements in the isolated subgroup). For this type of calculation, the subgroup to be isolated is considered to be one component, and the composition of this component is specified as the actual relative elemental composition of the subgroup to be isolated, but in terms of the altered elements. In order that these altered elements may equilibrate with each other, the species thermochemical data card set must contain a set of species which may be formed from these altered elements, i.e., species with the same atomic number convention.

5.3.5.4 Low Temperature Surface Equilibrium Suppression

As previously discussed, equilibrium is an increasingly poor assumption at low surface temperatures (e.g., below 2000°R) in some ablation problems. However, in most surface thermochemistry tables, lower temperature ranges are usually only of minor interest (e.g., during a very short initial period of a transient ablation problem). Nontheless, the surface tables must frequently extend to these lower temperatures in order to be compatible with the heat conduction and ablation solution. For these cases, the ACE package contains an option by which surface (heterogeneous) equilibrium will be suppressed and surface recession nulled ($\dot{m}_c = 0$) below some input limit temperature for solutions in the assigned temperature part of the surface tables. The gases adjacent to the surface are assumed to be in equilibrium, but heterogeneous equilibrium is not required for this solution. For many cases, surface thermochemistry tables generated in this fashion are closer to reality than full equilibrium solutions down to low temperatures. The input convention for implementing this option is discussed in Reference 2.

5.3.5.5 Full Treatment of Kinetics

The previous discussion has described various approximate treatments of kinetics effects which are often useful when a general solution, including an "exact" treatment of reaction rate effects, is either impossible or impractical. The ACE program does, however, possess the capability of accurately treating a number of kinetically controlled reactions in otherwise equilibrated systems (either closed or open). The remainder of this section

will be devoted to a brief description of this "exact" treatment of kinetics.

The inclusion of kinetically controlled chemical reactions is accomplished by removing equilibrium relations (39) from the set of equations for certain species participating in reactions that are to be kinetically controlled. These equations are replaced by kinetic rate equations (of the Arrhenius form) for each kinetically controlled reaction. This is accomplished by first identifying the primary reactive species in the reactions which are to be kinetically controlled, and second, by allowing these species to be created or destroyed only via the kinetic rate equations. This approach requires a relabeling of species to be considered in the kinetically controlled reactions. These species are called pseudo-elements since they behave like elements except that they may be created or destroyed at rates specified by the reaction rate equations.

Computationally, the inclusion of kinetics results in the addition of a rate-of-creation or destruction term to the elemental balance equations for these pseudo-elements. This adds additional unknowns tc the system equal in number to the number of species whose concentrations are kinetically controlled, i.e., the pseudo-elements. The relative creation and destruction rates of all pseudo-elements in a given reaction are related by stoichiometry, however, so the number of additional unknowns remaining is equal to the number of kinetically controlled reactions. The reaction rates, from which the pseudo-element creation or destruction rates derive, are given by

$$R_m = k_{Fm}\left[\prod_j P_j^{\mu_{jm}^R} - \frac{1}{K_{pm}}\prod_j P_j^{\mu_{jm}^P}\right] \qquad \text{moles/ft}^2\text{sec} \tag{72}$$

for each kinetically controlled reaction m of the form

$$\sum_j \mu_{jm}^R N_j \rightarrow \sum_j \mu_{jm}^P N_j \tag{73}$$

where the sums and products are over the species and pseudo-elements N_j, μ are the stoichiometric coefficients, and superscripts R and P denote reactants and products respectively. In (72), K_{pm} is the equilibrium constant for reaction (73), and k_{Fm} is the forward rate constant. In the

present formulation, k_{Fm} is represented by an Arrhenius type function

$$k_{Fm} = B_m T^{\phi_m} \exp\ (-E_m/RT) \tag{74}$$

where E_m is the activation energy, ϕ_m is the temperature exponent, and B_m is a constant representing a multitude of phenomena. E_m, ϕ_m, and B_m must be input to the program for each kinetically controlled reaction. These constants should be based on experimental data. The uncertainty in, or unavailability of, these data for many chemical systems of interest in ablation problems frequently represent a significant constraint on the application of the kinetics option of ACE program to these problems. More detailed discussion of the computational treatment of kinetics is presented in References 4 and 11. Reference 2 describes the input details for the kinetically controlled reaction data.

5.4 SOME CODING DETAILS

The computational procedures are employed in the ACE program to solve the equations set forth in Section 5.3, briefly discussed here. Considerably greater detail is presented in Reference 4 and in particular, Table I of that reference.

5.4.1 Basic Solution Technique

The basic solution technique may be illustrated by considering, for example, an open system with unequal diffusion coefficients, no condensed phase material removal, and no kinetics (i.e., as discussed in Section 5.3.3). For this system, the basic equations defining the problem are the elemental conservation equations (67), the total pressure equation (56), the reaction equilibrium equations (55), and one heterogeneous vapor pressure relation (53). The table of Section 5.3.3 shows that there are as many knowns as unknowns in these equations so closure is obtained.

Summarizing these equations,

$$B' \sum_{i=1}^{I} C_{ki} P_i + \bar{F} \sum_{i=1}^{I} C_{ki} P_i / F_i^{\gamma} - \frac{P \dot{m}_g}{\dot{m}_k} \left(\tilde{z}^*_{k_e} + B'_g \tilde{K}_{k_g} + B'_c \tilde{K}_{k_c} \right) = 0 \tag{75}$$

$$\sum_{i=1}^{I} P_i - P = 0 \tag{76}$$

$$\ell n\ P_i - \sum_{k=1}^{K} C_{ki}\ \ell n\ P_k - \ell n\ K_{pi}(T_w) = 0 \qquad (77)$$

$$- \sum_{k=1}^{K} C_{k\ell}\ \ell n\ P_k - \ell n\ K_{p\ell}(T_w) = 0 \qquad (78)$$

The number of unknowns could immediately be reduced by I-K through the direct substitution of (77), as solved for P_i, into the other relations. It proves advantageous, however, to continue to treat the full set of equations, and to subsequently utilize this substitution during the iterative convergence procedure. The solution of these simultaneous nonlinear algebraic equations is based on Newton-Raphson iteration. Since this procedure is accelerated by casting the equations into a more linear form (via transformations, substitutions, etc.) it is well to examine the set of equations above. With the boundary layer edge, char and pyrolysis gas composition given as well as the B', (75) and (76) are linear relations between the P_i and $\dot{m}_g$ providing that $\overline{F}$ is reasonably constant. In contrast, (77) and (78) are linear relations between the $\ell n\ P_i$, $\ell n\ P_k$ and $\ell n\ K_{pi}$, the latter variable being approximately linear in 1/T.

The ACE program takes advantage of this situation by treating those species which are significant in the mass and pressure balances (75) and (76) in terms of P_i and the less significant species in terms of their $\ell n\ P_i$.

The Newton-Raphson procedure, as applied by the ACE program, can be summarized by considering a set of equations of the general form

$$f_j(x_1, x_2, \ldots, x_i, \ldots) = 0$$

At any point in the solution procedure there exists a set of estimates, x_i^*, for all the variables which will in general not satisfy all of the relations and will lead to a non-zero value of the f_j, namely, ε_j. The Newton-Raphson method proceeds to "drive" these errors toward zero by evaluating the change in each unknown variable, Δx_i, which would reduce all the errors to zero if the functions, f_j, were linear. The linear approximation is based on the current values of the unknown variables and the corresponding array of values of the partial derivatives $\partial f_j / \partial x_i$.

Thus

$$df_j = \sum \frac{\partial f_j}{\partial x_i} dx_i \tag{79}$$

which is locally correct and is integrated to

$$(\Delta f_j)^* \approx \sum \left(\frac{\partial f_j}{\partial x_i}\right)^* (\Delta x_i)^* \tag{80}$$

in the linear approximation. The solution of (80) is

$$dx_i = \sum \frac{\partial x_i}{\partial f_j} df_j \tag{81}$$

where the array of partial derivatives appearing in (81) is simply the matrix inverse of the array in (80). In the ACE program the formulation of the partial derivatives uses the variables, $\ell n\ P_i$,† $\ell n\ T$ and $\ln \mathcal{M}$ and (81) yields, for example,

$$d(\ell n\ P_i) = \sum \frac{\partial\ \ell n\ P_i}{\partial f_j} df_j \tag{82}$$

which if taken as linear all the way to solution yields

$$\ell n \frac{P_i^{**}}{P_i^*} = (\Delta\ \ell n\ P_i)^* \approx \sum \left(\frac{\partial\ \ell n\ P_i}{\partial f_j}\right)^* (-\varepsilon_j)^* \tag{83}$$

since the desired change in the functions is simply the negative of the error. An equally exact relation obtained from (82) is

$$dP_i = P_i \sum \frac{\partial\ \ell n\ P_i}{\partial f_j} df_j \tag{84}$$

†The choice of $\ell n\ P_i$ permits a matrix reduction by the use of the simple algebraic substitution, previously mentioned after (78), prior to matrix inversion.

which if taken as linear all the way to solution yields

$$P_i^{**} - P_i^* = \Delta P_i^* \approx P_i^* \sum \left(\frac{\partial \ \ell n \ P_i}{\partial f_j} \right)^* (-\varepsilon_j^*) \tag{85}$$

The ACE program uses (85) for all species significant in mass balances and (83) for the others.

5.4.2 Restriction on Corrections

The set of correction $(\Delta x_i)^*$ can be thought of as a vector in the space of the independent variables which is added to the current vector approximation x_i^* to yield a new estimate x_i^{**} . Experience has shown that it is frequently unwise to proceed along this correction vector the full amount indicated by (83) or (85). Rather, it is better to proceed a limited way, although preserving the same direction. At other times, it is expedient to depart from this vector, and seek another based on freezing the value of some variable and eliminating a corresponding equation.

The scaling of the correction vector is such as to limit changes in the partial pressures of major species to increases of one order of magnitude and decreases of three orders of magnitude, and changes of temperature to approximately 20 percent.

Molecular weight, temperature and condensed phase concentration corrections are frozen and a new correction vector generated if the initial set of corrections indicate excessive temperature or molecular weight excursions, a contradictory temperature change, or negative corrections on newly introduced condensed species.

The formulation of these and other scaling and freezing criteria is an essential feature of the ACE program. Because of these features, convergence is virtually assured for well formulated, physically unique problems.

5.4.3 Base Species

The discussion of Section 5.3 described the equilibrium reaction equations as equations giving the formation of a species from atomic elements. Thus the reactants are elements and the products are usually molecules. This scheme has the advantage of formal simplicity, since the stoichiometric coefficients needed in the equilibrium equations are given directly by the

product species chemical formula. This scheme can have computational disadvantages, however, since the atomic elements are frequently not present to any great extent in the equilibrium system. This in itself results in no disadvantage. If, however, a molecule (e.g., CO) dominates more than one mass balance (e.g., C and O) ,loss of significant figures can slow or defeat convergence.

It is more desirable to write the equilibrium reactions (37) and (38) as well as the mass balances in terms of reactant species which are actually present in appreciable amounts. These species are termed "base species" (from Reference 12) since all other species are taken to be formed from them.

The ACE program selects the base species from the candidate species thermochemical data which are input as specified in Reference 2. The program automatically selects as base species the first set of species satisfying the requirement that (1) all other species may be formed from this base species set and (2) that no balanced reaction can be written involving only base species. One base species may be considered to represent each element. Thus, the base species are established by the order in which the user inputs the candidate species thermochemical data. The calculation of the stoichiometric coefficients and equilibrium constants appropriate to any set of base species is handled automatically by the program.

While the selection of base species is not usually critical, certain computational economies may be realized if the base species are those species which occur in relatively high concentrations in the system. Also the treatment of a chemical kinetics (Section 5.3.5) may have an influence on the selection of the base species. Therefore the Users' Guide (Reference 2) recommends certain input procedures for forcing the selection of desirable base species.

SECTION 6

COUPLING THE TRANSFER COEFFICIENT CALCULATION TO THE SURFACE THERMOCHEMISTRY SOLUTION (III - IV COUPLING) AND TO THE IN-DEPTH TRANSIENT SOLUTION (III - V COUPLING)

Section 5 above makes it plain that the transfer coefficient approach to modeling diffusional fluxes is built into the surface thermochemistry solution process, since the chemistry routines use B'_c as the measure of mass injection and the B'_c concept depends naturally on the transfer coefficient idea. An additional, more explicit, link to the transfer coefficient model is the scaling of kinetic effects on $\rho_e u_e C_M$. The pre-exponential factors B_m are input directly to the coupled code, and these are normalized on $\rho_e u_e C_M$ inside the ACE package, as noted in Section 5 above. This requires that a $\rho_e u_e C_M$ value be communicated directly to the ACE package with every call for use in normalizing and B_m's. Other coupling links appear in the surface temperature dependence and the "blowing reduction" of the transfer coefficient; these are discussed in Section 9 below.

The III - V coupling between the transfer coefficient and the in-depth solution occurs, of course, in the transfer coefficient equation for the surface energy events. The relevant equations have already been presented in Section 4.3 and require no further comment.

SECTION 7

COUPLING THE FLOW-FIELD (OR BOUNDARY LAYER EDGE STATE) SOLUTION (PHASE II) TO THE SURFACE STATE SOLUTION (II - IV COUPLING) AND TO THE TRANSFER COEFFICIENT SOLUTION (II - III COUPLING)

Before discussing the Phase II and III calculations themselves, it will be of interest to examine the coupling links between the Phase II solution, which refers to the specification of the boundary layer outer edge state around the body (pressure, static enthalpy, recovery enthalpy, and transport properties), and the Phase III and Phase IV solutions.

The boundary layer edge state influences the surface thermochemistry state solution, as has already been discussed in Section 5 above, through the direct communication of local pressure and recovery enthalpy to the ACE package. The edge state in turn is influenced by the current body shape, as will be discussed in Section 8 below.

The boundary layer edge state influences the transfer coefficient calculation through the distributions of pressure and enthalpy around the body, as might be expected. This is discussed in Section 9 below.

All of these coupling links are of interest, but it is also useful at times to be able to suppress some or all of them. Such coupling suppression is particularly desirable in parametric studies attempting to study one effect at a time, rather than coupled effects, and in studies in which it is desired to match experimental data in some respect (such as measured surface temperatures). Therefore, the MACABRE code has been written to allow varying degrees of decoupling. All of the following options exist for each surface point on a body at anytime:

a. Surface temperature and recession rate discovered by energy balance, or

b. Surface temperature and recession rate assigned as functions of time by user (Option 2)

Under (a) we have

a.1. Full surface energy balance with convection and thermochemistry (Option 1)

a.2. No convection, no recession, assigned heat flux (Option 3)

Under (a.1.) we have

a.1.1 Local pressure and/or local recovery enthalpy assigned by user as a function of time

a.1.2 Local pressure and/or local recovery enthalpy computed by appropriate subroutines automatically

For both (a.1.1) and (a.1.2) we have

a.1.($\frac{1}{2}$).1 Local heat transfer coefficient assigned by user as a function of time

a.1.($\frac{1}{2}$).2 Local heat transfer coefficient computed automatically by appropriate subroutines

For both (a.1.($\frac{1}{2}$).1) and (a.1.($\frac{1}{2}$).2) we have any degree of "blowing reduction" correction to the transfer coefficient.

SECTION 8

THE BOUNDARY LAYER EDGE STATE SOLUTION

A complete and accurate analysis of the boundary layer edge state is a very complex problem requiring simultaneous consideration of the body shape, shock shape, the shock layer flow, and the boundary layer flow. For many engineering purposes, however, a detailed analysis of this sort is not possible, and certain simplifying assumptions are necessary which bring the analysis to a more tractable level of sophistication. Since the application for the analytical technique being discussed here is primarily re-entry vehicle nosetips and heat shields, the first simplifying assumption is that the entire region of interest is immersed in a boundary layer edge flow which has passed through the detached bow shock at or near the stagnation point. Thus, it is not necessary to calculate a shock shape and shock layer flow since the shock layer gas of interest is assumed to pass through a normal shock. The next simplifying assumption is that the boundary layer edge gas state is determined by an isentropic expansion from the body stagnation condition. With the edge gas entropy fixed at the stagnation value, the complete edge gas thermodynamic state is determined by the specification of one more property, typically the local static pressure. Thus, the determination of the edge gas state reduces to a problem of first calculating the stagnation entropy, which is relatively straightforward, then determining the pressure distribution around the arbitrary body shape, and finally evaluating the other edge state properties of interest by carrying out the isentropic expansion to the known local pressure. The techniques used to carry out these steps are described in the subsections below.

8.1 THERMOCHEMICAL COMPUTATIONS

Thermochemical computations are required in a number of instances in the coupled code, including boundary layer edge state calculations. As mentioned in Section 5, these calculations are carried out by the ACE routine. For boundary layer gas properties, it has been found most convenient to store ACE solutions for the requisite thermodynamic and transport properties in tabular form and supply this table of properties to the program as input. The option also exists of merely specifying the desired values of the independent variables in this "Mollier Chart" and calling for ACE calculations to determine the required properties. The properties at the gas state of interest during the course of a solution are found by interpolation between tabular

values. The precalculated Mollier Chart approach has a number of advantages similar to the precalculated surface tables: reuseability, external evaluation of the table accuracy and sufficiency, and elimination of non-converged solutions. However, care must be taken to guarantee that interpolation within the chart will yield sufficiently accurate state properties.

The Mollier Chart uses pressure and enthalpy as independent variables. Dependent variables found at each (P-h) combination are temperature, density, Prandtl number, viscosity, entropy, and isentropic exponent. Linear interpolation is used everywhere within the chart, however pressures and densities are converted to logarithmic form before this linear interpolation is carried out. Since the computer code dimensions limit the number of pressure-enthalpy combinations which can be input, it is recommended that the user check the accuracy of interpolated solutions before going ahead with problem solving. This can be accomplished by plotting the properties of interest, determining the region of most likely error within the linear interpolation approximation, and comparing an interpolated point with an "exact" solution from the ACE program.

The edge state solution procedure is typically started by using the specified values of stagnation pressure and stagnation enthalpy to determine the entropy level from the Mollier Chart. The static pressure around the body must then be found, as discussed in the next section.

8.2 STATIC PRESSURE DISTRIBUTION

The technique used to calculate the static pressure distribution includes a variation of Newtonian theory in the subsonic flow near the stagnation point, matched to a Prandtl Meyer expansion downstream of the sonic point. The methods used in these regions are explained below.

8.2.1 Subsonic Region

The pressure distribution in the subsonic region is found by a variation of the technique suggested in Reference 13, in which the Newtonian pressure distribution relation is modified to include blunt bodies with sonic corners. The basic Newtonian pressure expression is

$$\bar{P} = \bar{P}_\infty + (1 - \bar{P}_\infty) \cos^2 \beta \qquad (86)$$

where barred quantities are normalized by the stagnation pressure, and β is the angle between the body axis of symmetry and a normal to the body surface at the point of interest. The sketch below will help to clarify this nomenclature.

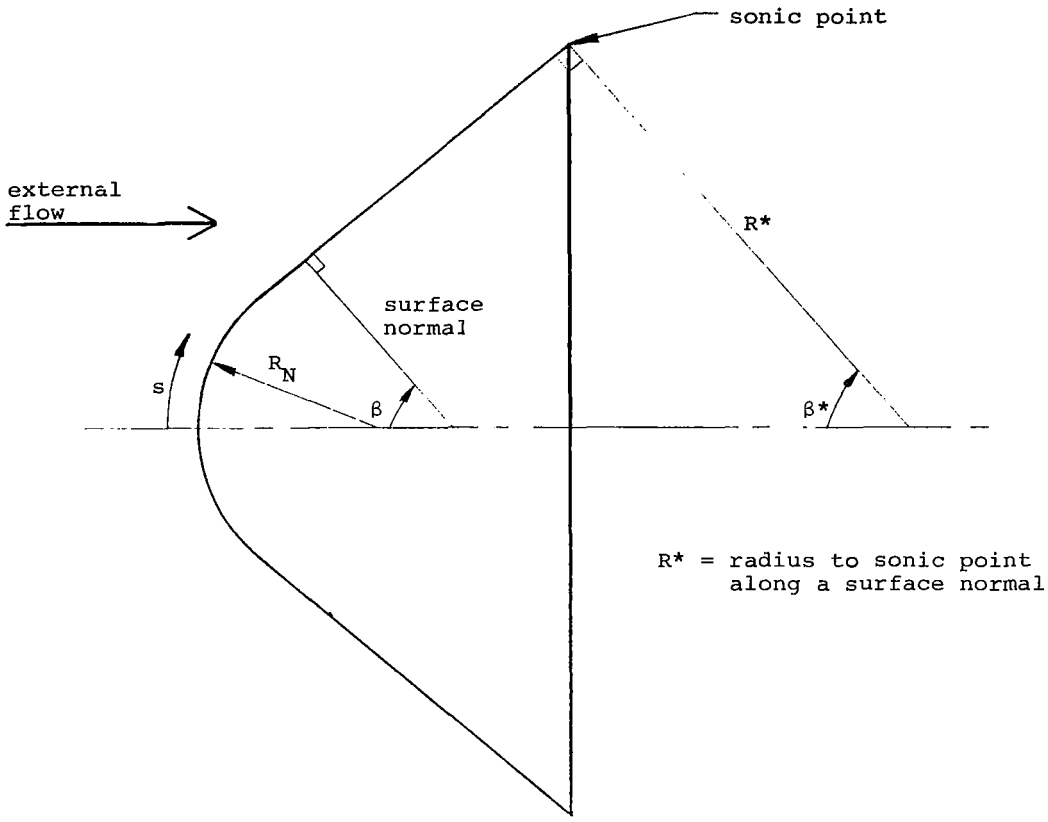

Figure 17. Diagram of Nosetip Showing Nomenclature

A class of nosetips of particular interest are smoothly contoured blunt bodies having local slopes such that the flow is subsonic everywhere ahead of a convex sharp corner and the flow expands to the supersonic condition at the corner. For these shapes, the Newtonian pressure distribution is grossly inaccurate since it depends only on local slope. It is obvious that the pressure should vary smoothly from the stagnation value $\overline{P} = 1.0$ at the stagnation point to the sonic point pressure $\overline{P} = \overline{P}^*$ at the sharp corner. However, for a sphere-cone shape as shown in Figure 17 above, the Newtonian description of pressure would call for a constant $\overline{P}$ determined by the surface slope along the entire cone surface. It was found in Reference 13 that a modification of the Newtonian distribution involving an empirical

expression for pressure on a flat disc of the same diameter (sonic point diameter) would greatly improve pressure predictions. The suggested pressure distribution expression, modified for nonzero ambient pressure, is

$$\bar{P} = \bar{P}_\infty + (1-\bar{P}_\infty)\cos^2\beta - (1-\bar{P}_{FD})\left(\frac{\cos^2\beta-\bar{P}^*}{1-\bar{P}^*}\right)$$

$$+ \left(1 - \frac{R_N}{R_{max}}\right)\left[(\sin^2\beta)\left(1-\frac{s}{s^*}\right) + \frac{1}{2}\frac{s}{s^*}\left[\bar{P}_{FD} - 1\right.\right.$$

$$\left.\left. + \frac{s}{s^*}(\sin^2\beta) + (1-\bar{P}_{FD})\left(\frac{\cos^2\beta-\bar{P}^*}{1-\bar{P}^*}\right)\right]\right] \qquad (87)$$

where $\bar{P}_{FD}$ is the flat disc pressure distribution expression, s is the surface running length, R_N is the nose radius, and R_{max} is the maximum of either the nose radius or R*, as defined in Figure 17. It is necessary to specify expressions for the sonic point pressure $\bar{P}^*$ and the flat disc pressure $\bar{P}_{FD}$ in order to use this expression. It is in this last expression that the present analysis differs from that of Reference 13.

The sonic point pressure has been chosen to be described by the ideal gas expression

$$\bar{P}^* = \left(\frac{2}{\gamma+1}\right)^{\frac{\gamma}{\gamma-1}} \qquad (88)$$

The isentropic exponent γ is evaluated at the stagnation point and is assumed to remain constant over the region of interest. The assumption of a constant γ introduces a negligibly small error into the analysis. Another quantity of interest is the location of the sonic point, s*. For the sharp cornered bodies discussed above, s* is merely the distance to the corner. However, as these sharp cornered bodies ablate or for other smoothly-contoured bodies, the sonic point must be located in order to use Equation (87). The Newtonian pressure distribution is employed here to give the surface angle at the sonic point of

$$\beta^* = \cos^{-1}\sqrt{\frac{\bar{P}^*-\bar{P}_\infty}{1-\bar{P}_\infty}} \qquad (89)$$

Thus the surface running length s* can be found by using the known surface

slopes and running lengths along the surface and interpolating between them.

The flat disc pressure distribution used in Reference 13 is

$$\bar{P}_{FD} = 1 - e^{-\lambda(1-\bar{P}^*)}$$

$$\lambda = 4\sqrt{\ell n\left(\frac{s^*}{s}\right)} \tag{90}$$

It will be shown that the heat transfer coefficient at the stagnation point depends upon the stagnation point velocity gradient (see Equation (120)). This gradient in turn depends upon the second derivative of pressure with distance according to the following relation

$$\left.\frac{du}{ds}\right|_{s\to o} = \sqrt{\left.-\frac{1}{\rho_o}\frac{d^2P}{ds^2}\right|_{s\to o}} \tag{91}$$

Differentiating Equation (87) twice yields

$$\left.\frac{d^2\bar{P}}{ds^2}\right|_{s\to o} = -\left(1-\bar{P}_\infty\right)\frac{2}{R_N R_{max}} + \frac{d^2\bar{P}_{FD}}{ds^2} \tag{92}$$

which for R_N approaching infinity yields a zero velocity gradient at the stagnation point if Equation (90) is employed as it stands. To correct this unrealistic result, the data of Reference 14 were evaluated to obtain a flat disc stagnation point velocity gradient expression

$$\left.\frac{du}{ds}\right|_{FD,s\to o} \approx \frac{1}{4s^*}\sqrt{\frac{2P_o}{\rho_o}} \tag{93}$$

By combining Equations (91), (92), and (93), the following result is obtained

$$\left.\frac{d^2\bar{P}}{ds^2}\right|_{s\to o} = \left(1-\bar{P}_\infty\right)\left(\frac{-2}{R_N R_{max}} - \frac{1}{8s^{*2}}\right) \tag{94}$$

This expression provides a more correct stagnation point pressure distribution The flat disc pressure distribution, Equation (90), has been modified to blend smoothly with the new second derivative requirements,

$$\bar{P}_{FD} = 1 - e^{-\lambda}(1-\bar{P}^*) - \frac{1}{16}\left[\left(\frac{s}{s^*}\right)^2 - e^{-\lambda}\right] \qquad (95)$$

and the definition of λ has been changed slightly:

$$\lambda = 5\sqrt{\ell n(\frac{s^*}{s})} \qquad (96)$$

Equations (95) and (96) are the final forms of the flat disc pressure distribution relations which are used in the present analysis.

8.2.2 Downstream of the Sonic Point

Using the expression given in Equation (87) above, the local static pressure is exactly equal to the Newtonian pressure for all body shapes at the sonic point. The Newtonian description of pressure is then used downstream of the sonic point until the Prandtl-Meyer match point is reached, at which point a Prandtl-Meyer expansion expression is used for the remainder of the running length. The match point is determined by the requirement of continuity of pressure and pressure gradient along the surface:

$$\left.\frac{dP}{ds}\right|_{Newtonian} = \left.\frac{dP}{ds}\right|_{Prandtl\text{-}Meyer} \qquad (97)$$

It is more convenient to work in terms of the angle β and dimensionless pressure:

$$\left.\frac{d\bar{P}}{d\beta}\right|_{Newtonian} = \left.\frac{d\bar{P}}{d\beta}\right|_{Prandtl\text{-}Meyer} \qquad (98)$$

The Newtonian pressure expression can be differentiated to give

$$\left.\frac{d\bar{P}}{d\beta}\right|_{Newtonian} = -(1-\bar{P}_\infty)\sin 2\beta \qquad (99)$$

For a perfect gas, the Prandtl-Meyer pressure gradient is

$$\left.\frac{d\bar{P}}{d\beta}\right|_{\text{Prandtl-Meyer}} = -\frac{\gamma \bar{P} M^2}{\sqrt{M^2-1}} \tag{100}$$

while the relation between pressure and Mach number is

$$\bar{P} = \left(1 + \frac{\gamma-1}{2} M^2\right)^{\frac{\gamma}{1-\gamma}} \tag{101}$$

Equating the two gradient expressions yields the following equation for the match point:

$$\beta_M = \frac{1}{2} \sin^{-1}\left\{ \frac{\bar{P}\gamma M^2}{(1-\bar{P}_\infty)\sqrt{M^2-1}} \right\} \tag{102}$$

This is an implicit equation for β_M, since $\bar{P}$ and M are functions of β. The solution is found by a Newton-Raphson iteration procedure.

Pressures on the body downstream of the match point are found by carrying out a Prandtl-Meyer expansion from the match point conditions to the local surface slope. The governing equations in this region are Equation (101) above relating pressure to Mach number, and

$$\beta = \beta_M + \sqrt{\frac{\gamma+1}{\gamma-1}} \tan^{-1}\sqrt{\frac{\gamma-1}{\gamma+1}(M^2-1)} - \tan^{-1}\sqrt{M^2-1} - \sqrt{\frac{\gamma+1}{\gamma-1}} \tan^{-1}\sqrt{\frac{\gamma-1}{\gamma+1}(M_M^2-1)} + \tan^{-1}\sqrt{M_M^2-1} \tag{103}$$

which relates Mach number to local surface angle. Once again, the equations are implicit since M is a function of β, therefore a Newton-Raphson iteration procedure was devised to solve these equations.

8.2.3 Examples of the Accuracy of the Method

The accuracy of the pressure prediction technique described above is demonstrated with four sample problems. The first of these is a 60° half angle sphere cone with a sharp corner as shown in Figure 18. With this shape, the location of the sonic point is fixed at the sharp corner, therefore β^*, s^*, and R_{max} are known from the geometry. The pressure prediction for this shape is compared in Figure 18 to the data of Reference 15, and also to the Newtonian pressure distribution for the same shape. Agreement is seen to be excellent over most of the surface, which is to be expected since the empirical portions of the theory were invented to solve this very problem. The shortcomings of Newtonian theory are also readily apparent in this figure.

Figure 19 demonstrates the utility of this pressure prediction technique on a spherical shape. For spheres, the Newtonian description of pressure in the subsonic region is generally very good, and this case is no exception. The differences between Newtonian and the currently proposed theory on a sphere in the subsonic region are very slight, however, and both methods give good agreement with the experimental data.

Figures 20 and 21 demonstrate the agreement between theory and experiment for a blunt and a sharp ellipse, respectively. Again, there is very little difference between Newtonian and the current theories, with either giving satisfactory agreement with the data.

In summary, the present theory offers good agreement with Newtonian theory for spherical and elliptical shapes, but also provides accurate descriptions of pressure over flat-disc-type shapes where Newtonian theory fails entirely. This makes the theory particularly suitable for the large cone angle blunt shapes being considered for planetary entry.

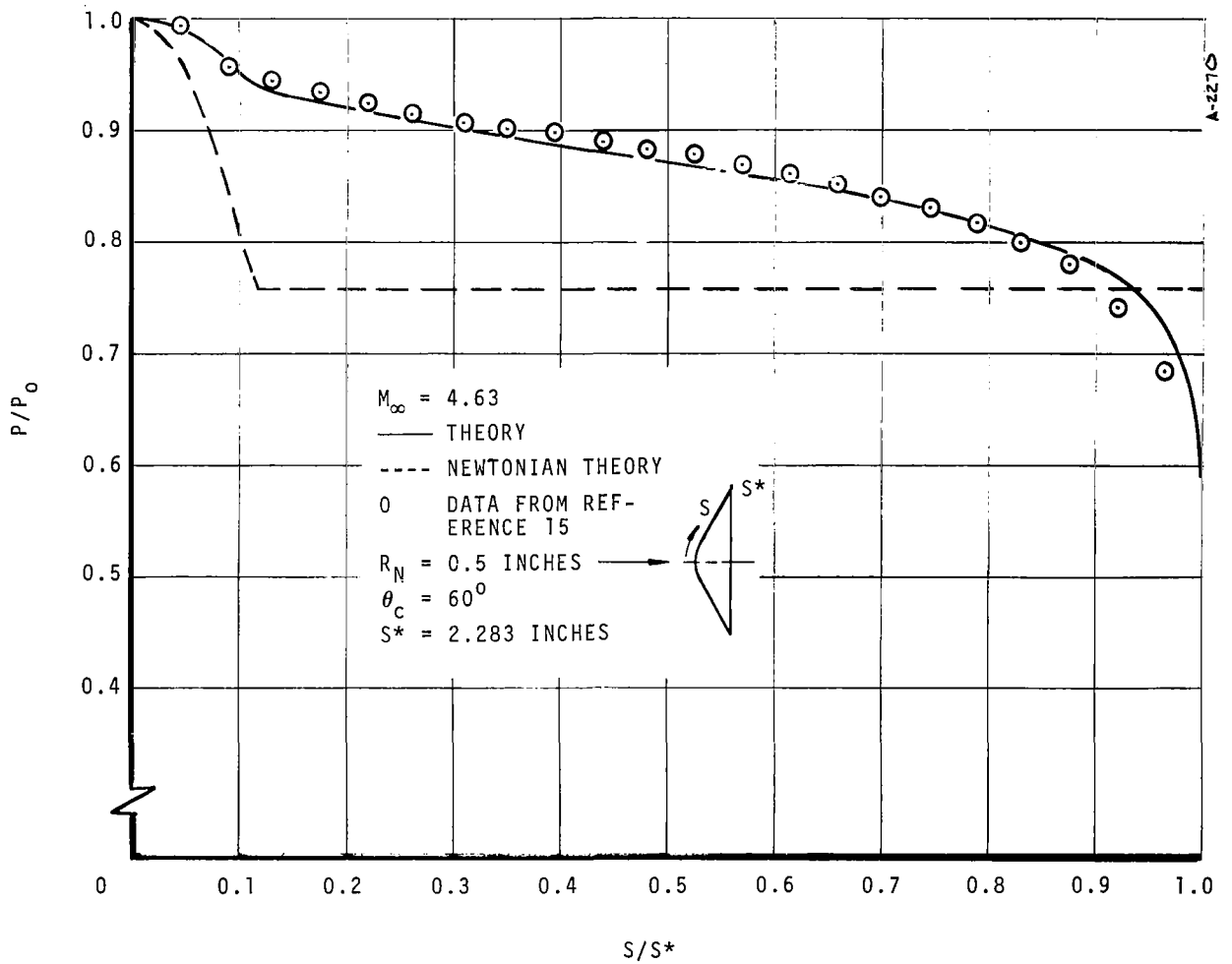

Figure 18. Pressure Distribution on a 60° Sphere Cone with Sonic Corner

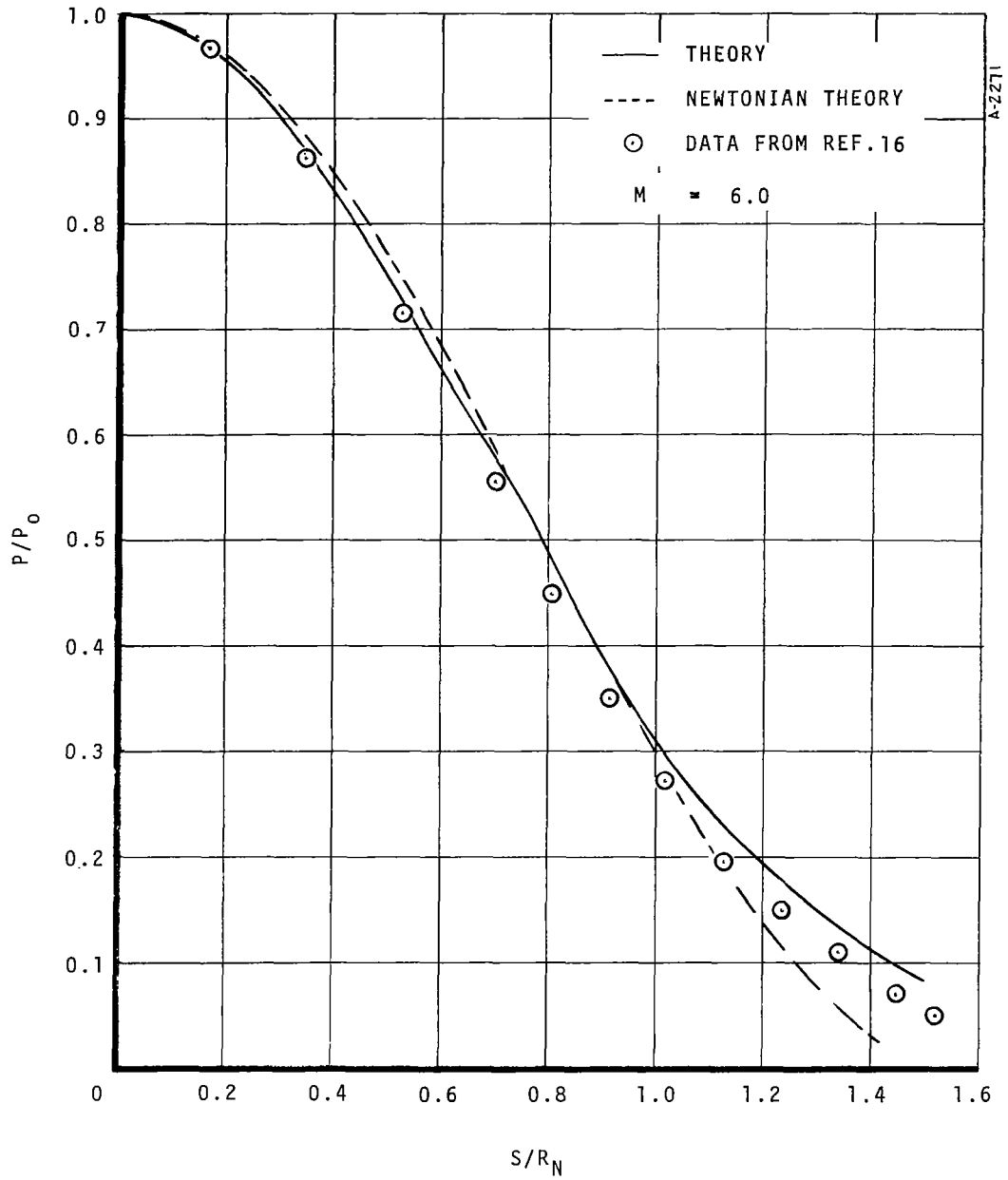

Figure 19. Pressure Distribution on a Sphere

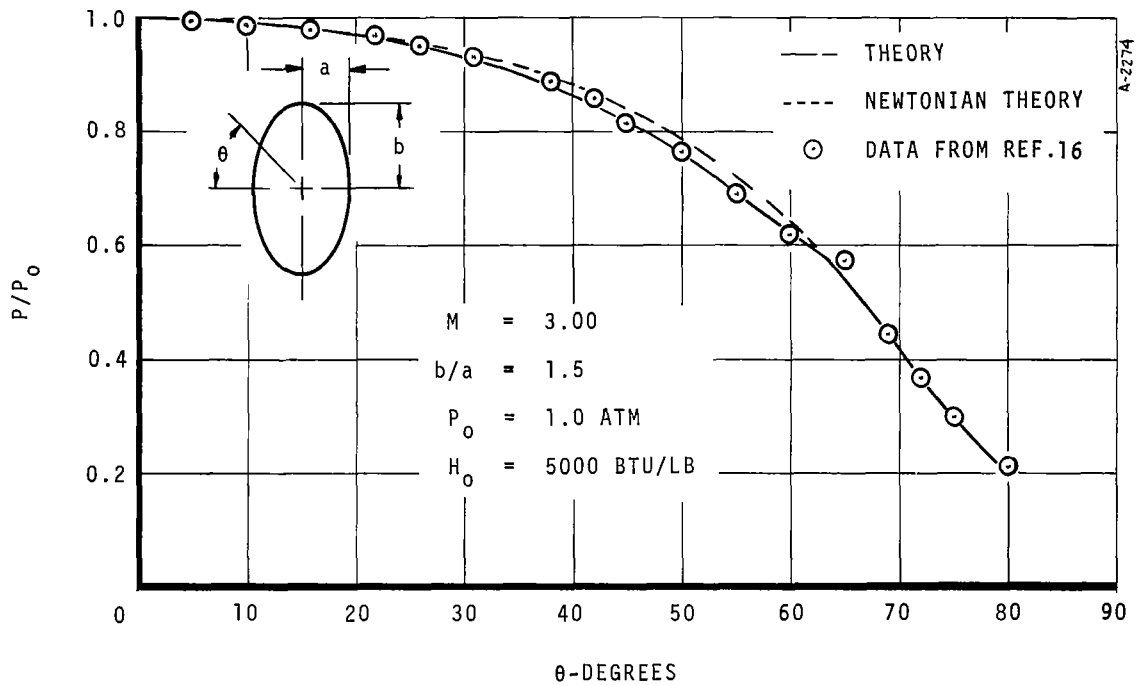

Figure 20. Pressure Distribution on an Ellipse

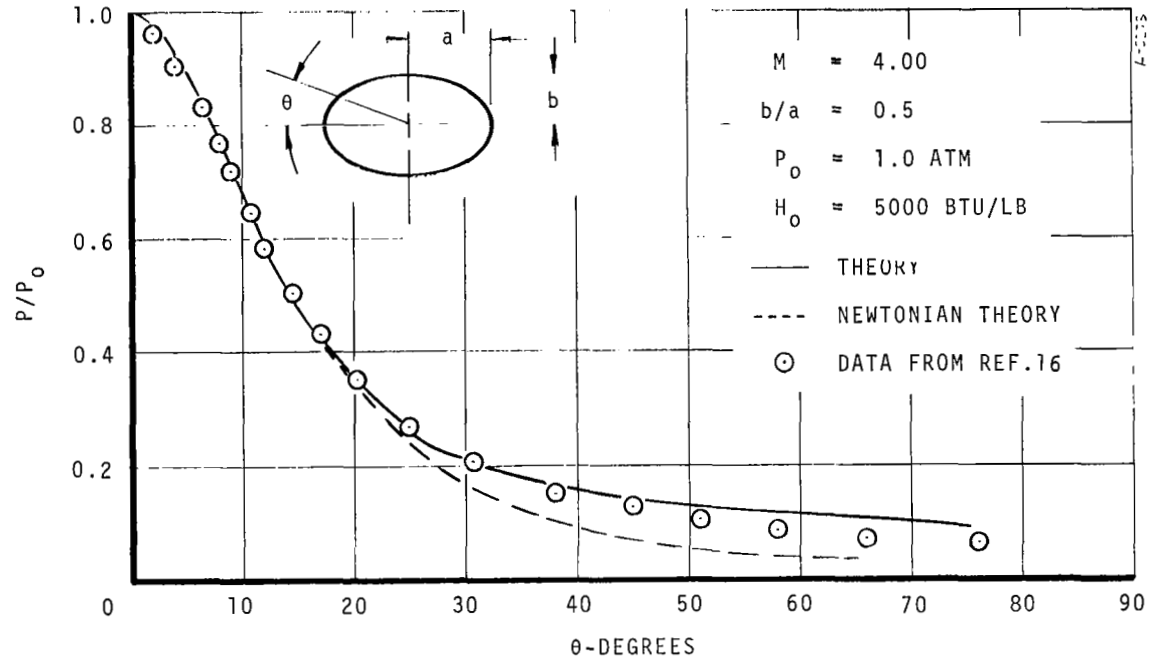

Figure 21. Pressure Distribution on an Ellipse

8.3 EVALUATION OF OTHER PROPERTIES

Once the pressure is known at any given body point and the entropy is assumed equal to the stagnation value, other gas properties of interest may be found by referring to the Mollier Chart tables as described in Section 8.1. Some care is necessary in carrying out this operation, however. The Mollier Chart lookup subroutines have been written to use pressure and enthalpy as the independent variables in the lookup procedure since these are the known quantities at the stagnation point. In order to minimize the error resulting from linear interpolation, properties at other body points where pressure and entropy are known are found iteratively by estimating enthalpy, looking in the tables at the known P and estimated h, determining entropy s, comparing with the known s, revising the h estimate, and so on. This procedure prevents a compounding of errors which could arise if one were to interpolate on P and h to find s, then interpolate P and s to find h.

SECTION 9

THE TRANSFER COEFFICIENT EVALUATION

An energy integral technique is used to evaluate the nonablating heat transfer coefficient along the surface of an arbitrary body shape which starts at a stagnation point. The energy integral technique is completely discussed in Reference 17, and will be only briefly summarized here.

In the energy integral technique, the flat plate relationship between energy thickness and heat transfer rate is assumed to be valid for all types of flows. This relationship is then utilized to solve the energy integral equation for an arbitrary flow. To outline this method, it is useful to establish a few basic definitions.

heat transfer coefficient:

$$C_H' \equiv \frac{q_w}{\rho' u_e (H_r - h_w)} \tag{104}$$

energy thickness:

$$\phi \equiv \frac{H_r - h_w}{H_e - h_w} \int_o^\delta \frac{\rho u}{\rho_e u_e} \left(\frac{H_e - H}{H_r - h_w} \right) dy \tag{105}$$

$$\bar{\phi} = \phi \left(\frac{H_e - h_w}{H_r - h_w} \right) \tag{106}$$

reference enthalpy:

$$h' = 0.23 h_e + 0.19 H_r + 0.58 h_w \quad \text{(laminar)}$$

$$h' = 0.36 h_e + 0.19 H_r + 0.45 h_w \quad \text{(turbulent)} \tag{107}$$

where

$$H_r = h_e + \tilde{r} \frac{u_e^2}{2} \tag{108}$$

$$\left.\begin{aligned} \tilde{r} &= (Pr')^{1/2} \text{ (laminar)} \\ \tilde{r} &= (Pr')^{1/3} \text{ (turbulent)} \end{aligned}\right\} \tag{109}$$

and all primed quantities are evaluated at the reference enthalpy condition.

It will be recalled that for flat plate flows with no initial boundary layer, the heat transfer coefficient expression is

$$C_H' = \frac{a}{(Pr')^{2/3}\left(\frac{\rho' u_e x}{\mu'}\right)^m} \tag{110}$$

where $a = 0.332$, $m = 0.5$ } laminar

or $a = 0.0296$, $m = 0.2$ } turbulent

Combining this with the definition of C_H' results in

$$\frac{q_w}{\rho_e u_e (H_r - h_w)} = \frac{a(\rho')^{1-m}(\mu')^m}{\rho_e u_e^m x^m (Pr')^{2/3}} \tag{111}$$

which relates heat flux to x for a flat plate. For the flat plate with nearly isothermal walls, the energy integral equation is

$$\frac{d\bar{\phi}}{dx} = \frac{q_w}{\rho_e u_e (H_r - h_w)} \tag{112}$$

Combining Equations 111 and 112 and assuming small variation in h_w compared with $H_r - h_w$, the flat plate energy integral equation can be solved to yield a relationship between energy thickness and x:

$$x = \left[\frac{(Pr')^{2/3}\left(\frac{\rho' u_e}{\mu'}\right)^m (1-m)\bar{\phi}}{a(\rho'/\rho_e)}\right]^{1/1-m} \tag{113}$$

By combining Equations 113 and 111, we have an explicit relationship between heat flux and energy thickness:

$$\frac{q_w}{\rho_e u_e (H_r - h_w)} = \left[\frac{a(\rho'/\rho_e)}{(Pr')^{2/3}\left(\frac{\rho' u_e \bar{\phi}}{\mu'}\right)^m (1-m)^m}\right]^{\frac{1}{1-m}} \tag{114}$$

This expression is now assumed to be valid for planar bodies or bodies of revolution, with arbitrary pressure gradient.

The more general boundry layer energy equation in integral form is

$$\frac{d\bar{\phi}}{dx} + \left[\frac{1}{r\rho_e u_e}\frac{d}{dx}(r\rho_e u_e) + \frac{1}{(H_r-h_w)}\frac{d}{dx}(H_r-h_w)\right]\bar{\phi} = \frac{q_w}{\rho_e u_e (H_r-h_w)} \tag{115}$$

Combining Equations 115 and 114 , the resulting form ca. e integrated directly to give

$$\bar{\phi}^{\frac{1}{1-m}} = \left\{\frac{\left[r\rho_e u_e (H_r-h_w)\right]_i}{r\rho_e u_e (H_r-h_w)}\bar{\phi}_i\right\}^{\frac{1}{1-m}} + \frac{1}{\left[r\rho_e u_e (H_r-h_w)\right]^{\frac{1}{1-m}}}\int_{x_i}^{x}\left[\frac{ar\rho' u_e (H_r-h_w)(\mu')^m}{Pr^{2/3}(\rho' u_e)^m (1-m)^m}\right]^{\frac{1}{1-m}}\frac{d\lambda}{(1-m)} \tag{116}$$

where λ is a dummy variable representing running length. This relation between $\bar{\phi}$ and x can be combined with Equation 114 above to give the general relation between heat flux (or heat transfer coefficient) and x. For laminar flows starting from a stagnation point, the final expression is

$$\rho_e u_e C_H = \frac{0.332\rho'\mu' r u_e (H_r-h_w)}{(Pr')^{2/3}\left\{\int_o^x r^2\rho'\mu' u_e (H_r-h_w)^2 d\lambda\right\}^{1/2}} \tag{117}$$

Similarly, for all turbulent flow,

$$\rho_e u_e C_H = \frac{0.0296\ \rho' u_e (\mu' r)^{1/4}(H_r-h_w)^{1/4}}{(Pr')^{2/3}\left\{\int_o^x \rho' u_e (\mu')^{1/4} r^{5/4}(H_r-h_w)^{5/4} d\lambda\right\}^{1/5}} \tag{118}$$

Finally, for transition from laminar to turbulent flow at $x = x_t$,

$$\rho_e u_e C_H = (0.0129\ 'u_e(\mu' r)^{1/4}(H_r - h_w)^{1/4} \Bigg/ \left[(Pr')^{5/6}\left\{0.9028\left(\int_o^{x_t}\frac{r^2}{(Pr')^{4/3}}\rho'\mu' u_e (H_r - h_w)^2 d\lambda\right)^{1/8} + 0.0161\int_{x_t}^{x}\frac{r^{5/4}}{(Pr')^{5/6}}\rho' u_e (\mu')^{1/4}(H_r - h_w)^{5/4} d\lambda\right\}^{1/5}\right] \tag{119}$$

For a stagnation point, we use the laminar expression and take the limit as $x \to o$ with

$$r = x$$

$$u_e = \left(\frac{du_e}{dx}\right) x$$

$$\rho'\mu' = \text{const.}$$

$$H_r - h_w = \text{const.}$$

The heat transfer coefficient reduces to

$$\rho_e u_e C_H = \frac{0.664}{(Pr')^{2/3}} \left[\rho'\mu' \left.\frac{du_e}{dx}\right|_o\right]^{1/2} \tag{120}$$

Consistent with the pressure distribution discussed in Section 8.2.1, the stagnation point velocity gradient can be expressed as

$$\left.\frac{du}{ds}\right|_{s=o} = \left[-\frac{1}{\rho}\frac{d^2P}{ds^2}\right]_{s=o}^{1/2} \tag{121}$$

which becomes

$$\left.\frac{du}{ds}\right|_{s=o} = \left\{\left(\frac{P_o - P_\infty}{\rho_o}\right)\left(\frac{2}{R_N R_{max}} + \frac{1}{8s^{*2}}\right)\right\}^{1/2} \tag{122}$$

In the present version of the code, only the laminar heat transfer expression, Equations (117) and (120), are included. For programming purposes, it is most convenient to write the heat transfer expression in the form

$$\rho_e u_e C_H = \frac{0.332}{(Pr')^{2/3}} (\rho'\mu')^{1/2} \left(\frac{u^*}{\ell^*}\right)^{1/2} \tag{123}$$

where

$$\frac{u^*}{\ell^*} = 4\frac{du_e}{ds} \quad \begin{pmatrix}\text{stagnation}\\ \text{point}\end{pmatrix} \tag{124}$$

or

$$u^* = u_e \qquad \left.\begin{array}{l}\\ \\ \end{array}\right\} \text{away from stagnation point} \tag{125}$$

$$\ell^* = \frac{\int_0^s \rho'\mu'(H_r - h_w)^2 r^2 u_e ds}{\rho'\mu'(H_r - h_w)^2 r^2 u_e} \tag{126}$$

The running integral term for ℓ^* away from the stagnation point is evaluated by treating each linear term in the integrand as if it varied linearly between body stations where its value is known. That is, ρ', μ', $H_r - h_w$, r, and u_e are all approximated as linear functions of s between each pair of body stations, thus making direct integration possible. The value of the integral at each body station is stored and merely added to the increment in ℓ^* at each new body station. All primed quantities are evaluated by referring to the Mollier Chart lookup routine with the known pressure and reference enthalpy.

An example of the accuracy of the energy integral method is provided in Figure 22, where results of the present theory applied to a sphere-cone configuration are compared with results from Aerotherm's multicomponent, nonsimilar, boundary layer analysis program (Reference 18). The two programs were supplied with identical pressure and wall temperature distributions over the length of interest. It is apparent that the energy integral approach gives satisfactory results for the nonablating heat transfer coefficient for at least a sphere-cone type of body.

For use in the MACABRE code, the nonablating heat transfer coefficients computed with the analysis outlined above are corrected to account for the effects of ablation ("blowing"). If we denote this nonablating coefficient (that is, for $\dot{m} = 0$) as $\rho_e u_e C_{H_0}$, then both data and simple analyses (see, for example, Reference 7) indicate that the dependence of $\rho_e u_e C_H$ on $\dot{m}$ is given fairly accurately by

$$\frac{C_H}{C_{H_0}} = \frac{\varphi}{e^{\varphi} - 1} \tag{127}$$

where

$$\varphi = \frac{2\lambda \dot{m}}{\rho_e u_e C_{H_0}} \tag{128}$$

This correction is built into the surface energy balance operations of the MACABRE code.

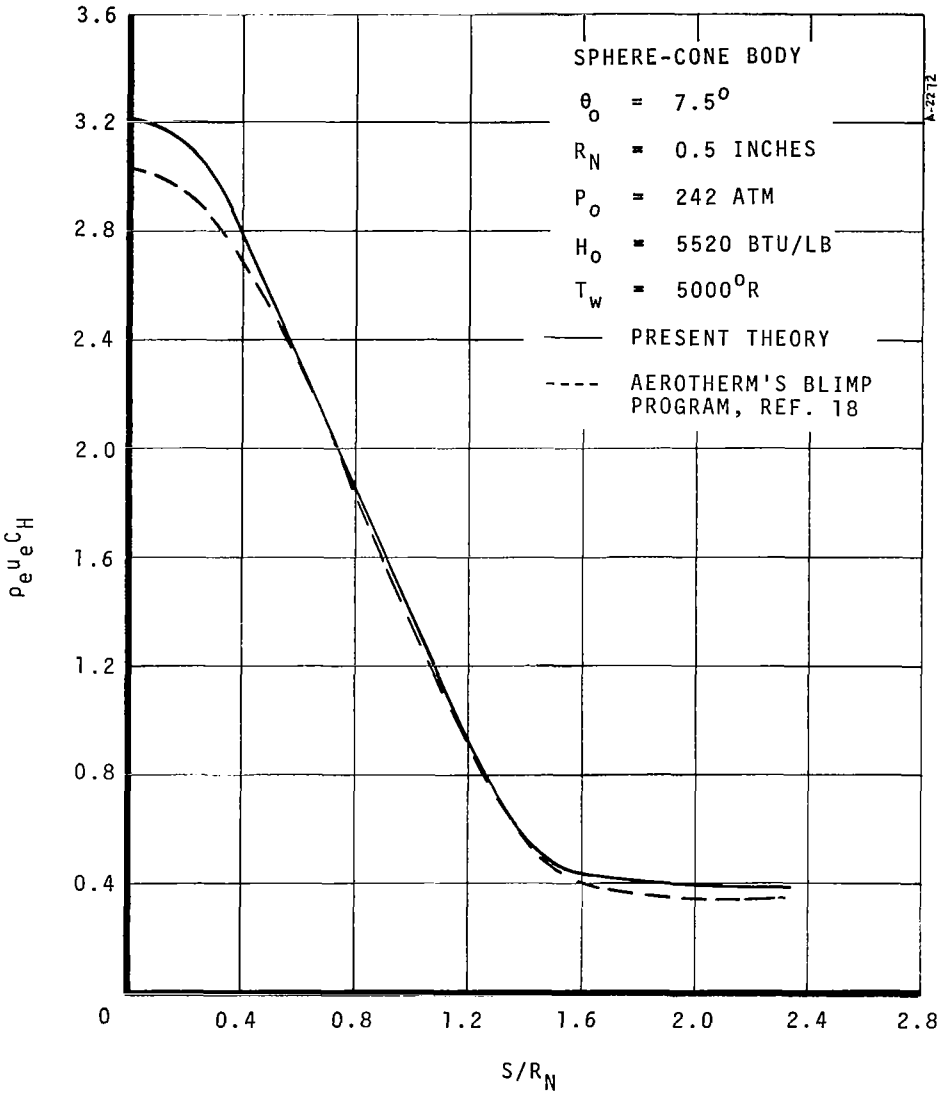

Figure 22. Heat Transfer Coefficient Prediction

SECTION 10

OVERVIEW OF COMPUTER PROGRAM EVENTS

The preceding sections have described the individual computing phases of the coupled computer code and the linkages between the phases. This section presents two simple flow charts for the code to clarify further the operation of the code. Figure 23 gives an overall chart of code events, and Figure 24 shows some details of the surface energy balance sub-package.

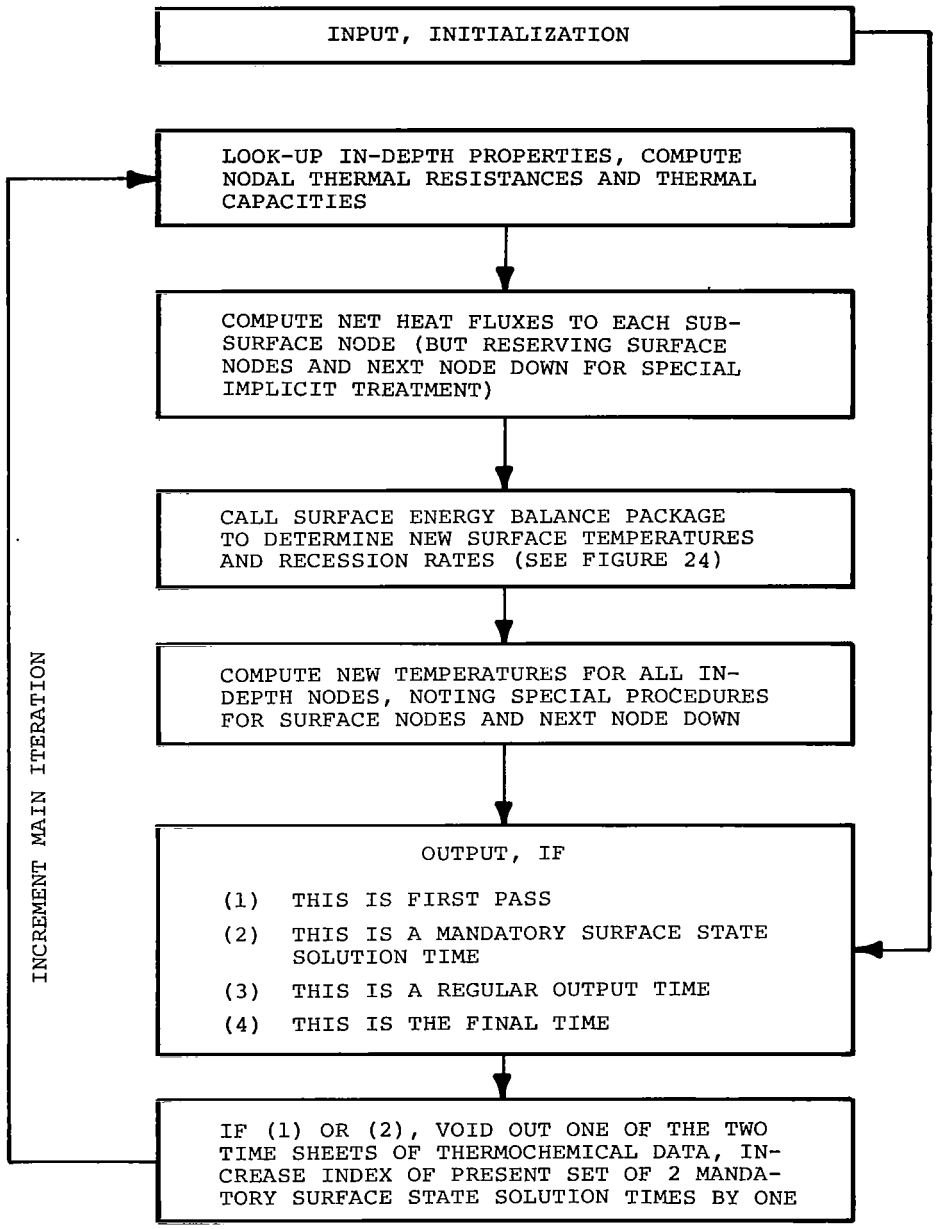

Figure 23. Overall MACABRE Code Flow Chart

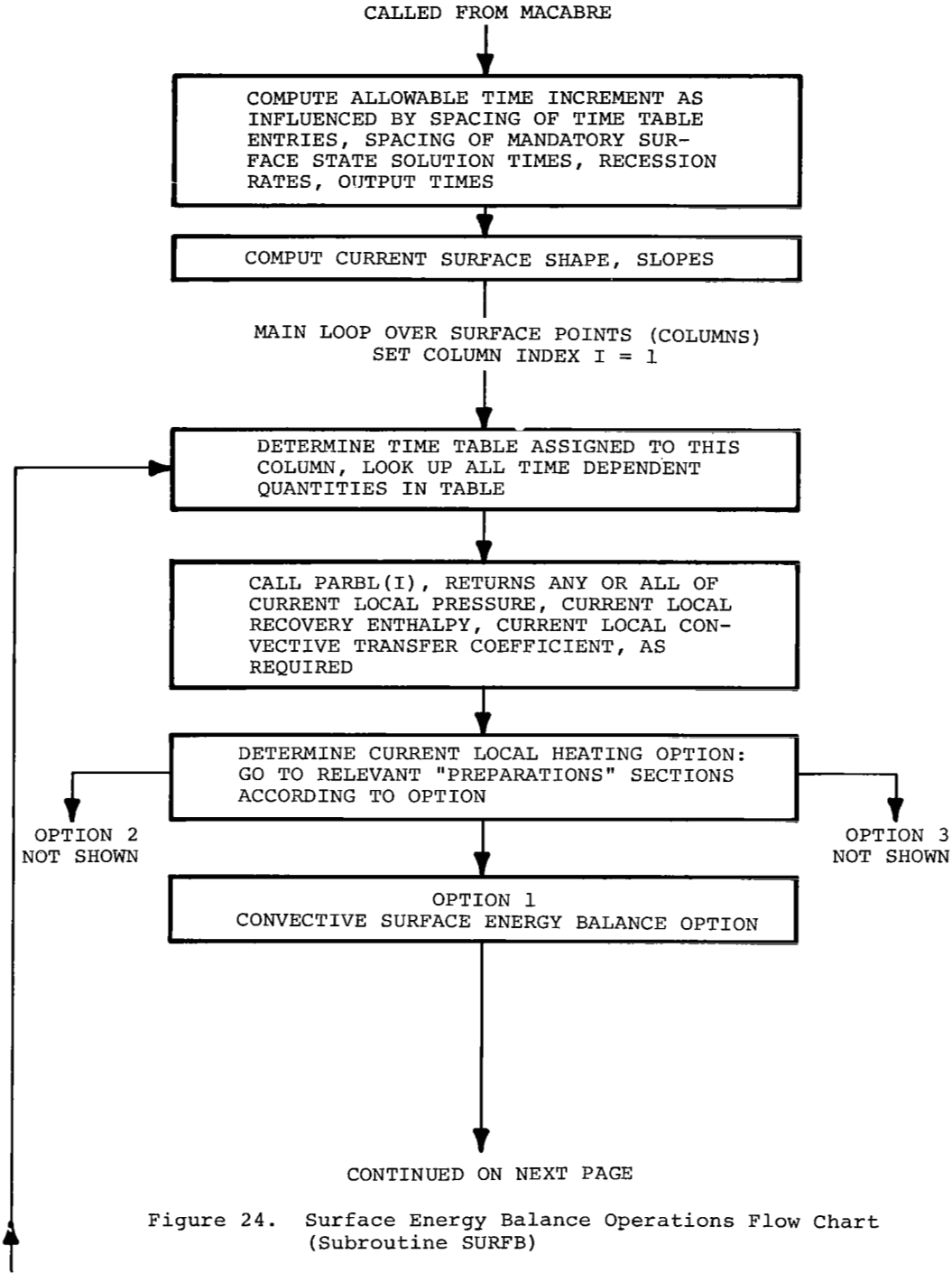

Figure 24. Surface Energy Balance Operations Flow Chart (Subroutine SURFB)

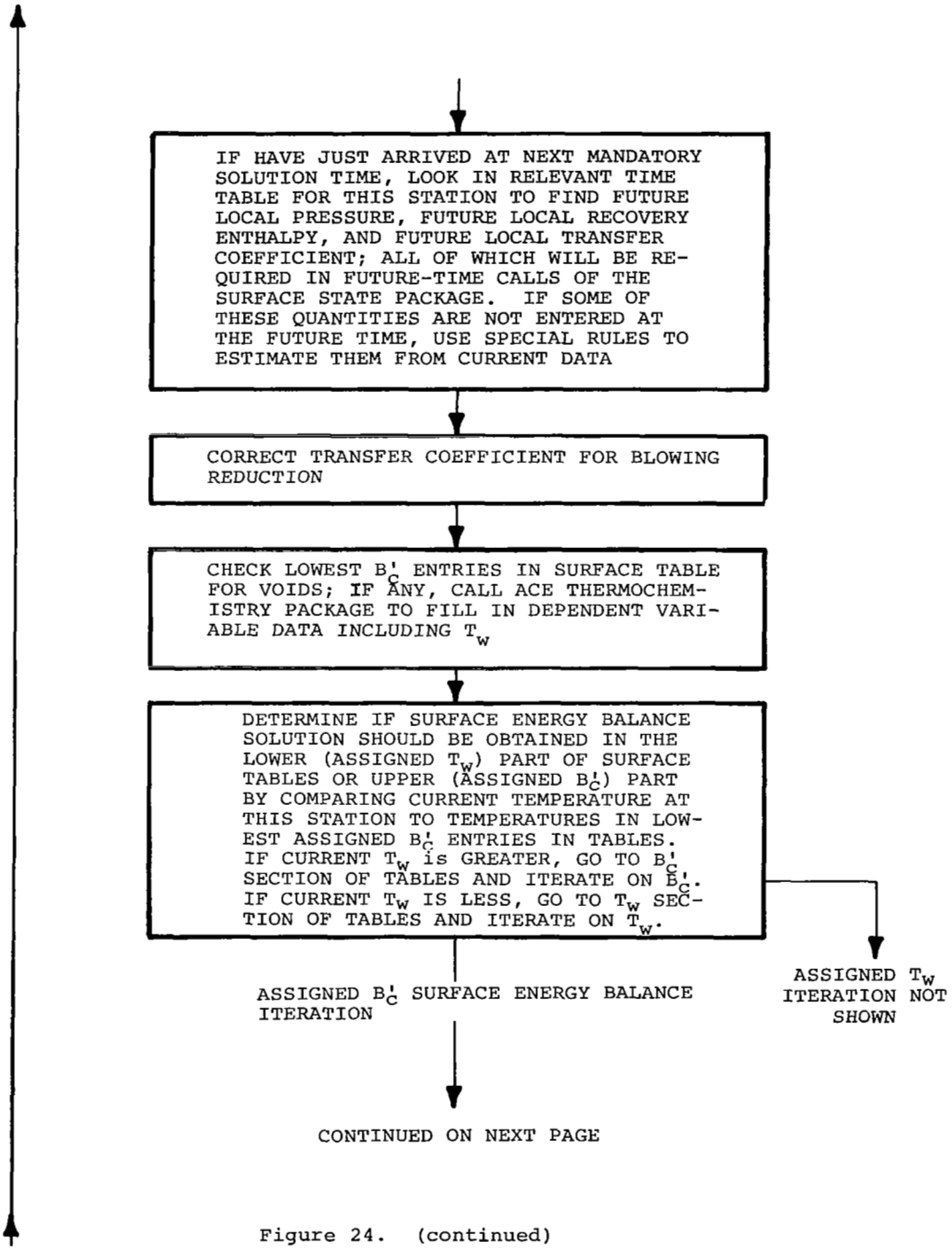

Figure 24. (continued)

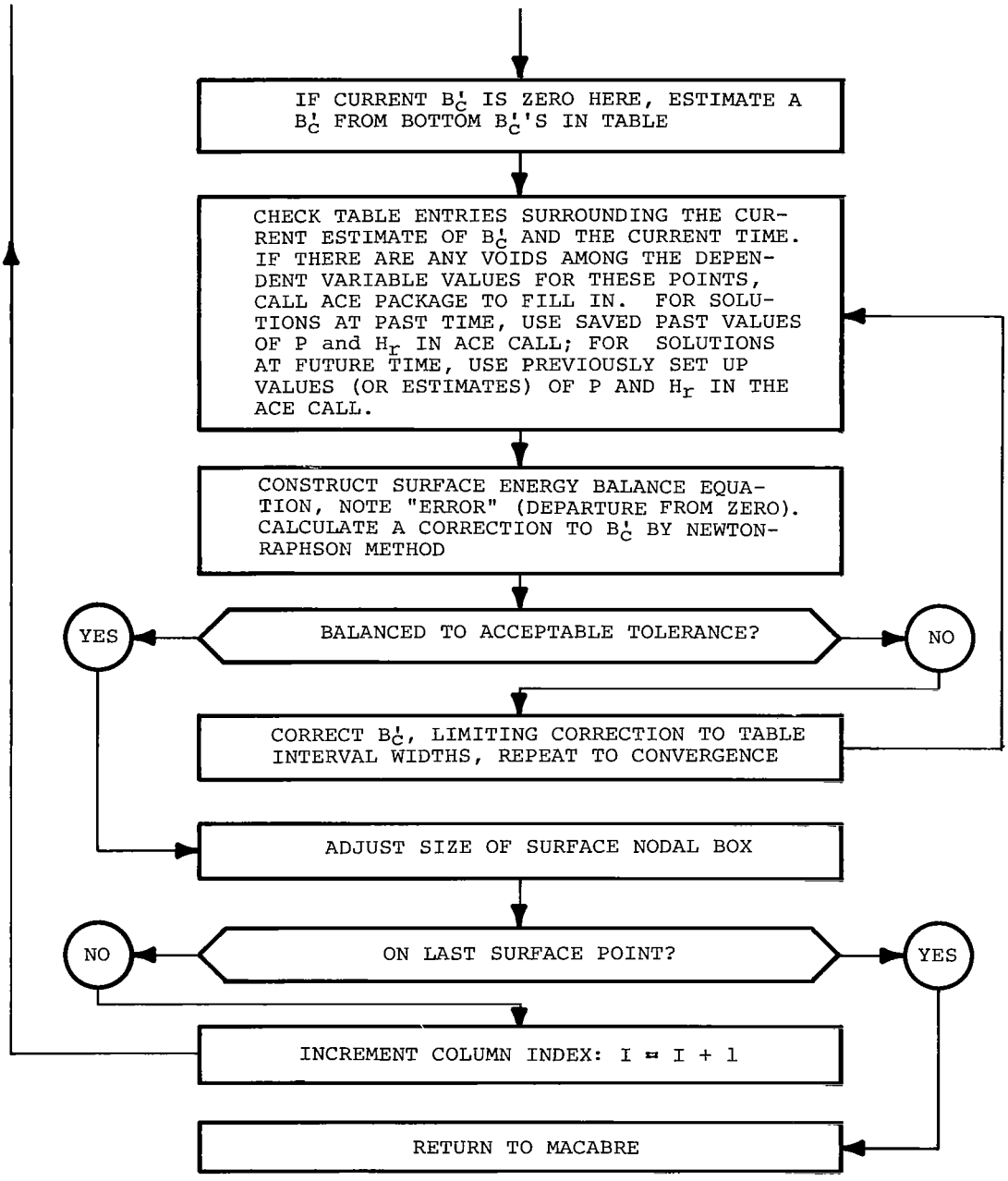

Figure 24. (concluded)

APPENDIX A

TRANSPORT PROPERTIES FROM THE ACE PACKAGE

When the ACE package of subroutines is used to generate transport property data for subsequent use in the transfer coefficient subroutine RUCH, the transport properties are calculated by ACE from expressions which derive from simple kinetic theory and the particular multicomponent diffusion representation previously discussed in Section 5.3.3. The development of these expressions is discussed in detail in Reference 19. A brief summary of this development, and the resulting expressions, are presented in this section.

Diffusion Coefficients - In Section 5.3.3, a bifurcation approximation for binary diffusion coefficients was mentioned which characterized multicomponent diffusion phenomena with reasonable accuracy without unduly complicating the system of equations to be solved. This simplification is achieved through a correlation for binary diffusion coefficients of the form

$$\mathcal{D}_{ij} = \frac{\bar{D}}{F_i F_j} \tag{A-1}$$

where $\bar{D}$ is a reference diffusion coefficient and the F_i are diffusion factors. These quantities are discussed in detail in Reference 19. The incorporation of (A-1) in the Stefan-Maxwell relation for mass diffusion fluxes indicates that the diffusion flux of species i may be written in terms of only properties of species i and global system properties. Subject to a few simplifying assumptions (Reference 19), this expression for j_i may be written

$$j_i = \frac{\rho \bar{D} \mu_2}{\mu_1} \frac{\partial z_i}{\partial y} \tag{A-2}$$

where

$$z_i = \mathcal{M}_i x_i / F_i \mu_2 \tag{A-3}$$

$$\mu_1 = \sum_j x_j F_j \tag{A-4}$$

$$\mu_2 = \sum_j \mathcal{M}_j x_j / F_j \tag{A-5}$$

The accuracy of this formulation is examined in Reference 19 for a variety of chemical systems. It is shown that the $\mathcal{D}_{ij}$ calculated by Equation (A-1) represent a very substantial improvement over equal diffusion coefficients when compared to exact values calculated directly from kinetic theory. The calculation of the mixture viscosity and thermal conductivity is based on the diffusion factors given by (A-1), and these will be discussed in the following paragraphs.

Mixture Viscosity - The expression employed by the ACE program to calculate the mixture viscosity derives from rigorous first order kinetic theory (Reference 20), subject to a few simplifying assumptions, as discussed in Reference 19.

$$\mu_{mix} = \sum_{i=1}^{I} \left[\frac{x_i \mu_i}{x_i + 1.385 \frac{RT\mu_i}{P\mathcal{M}_i} \sum_{\substack{j=1 \\ j \neq i}}^{I} \frac{x_j}{\mathcal{D}_{ij}}} \right] \tag{A-6}$$

where μ_i is the viscosity of the pure species i. The μ_i may be expressed in terms of the self diffusion coefficients $\mathcal{D}_{ii}$

$$\mu_i = \frac{5}{6A^*_{ii}} \rho_i \mathcal{D}_{ii} \tag{A-7}$$

where A^*_{ii} is a ratio of collision integrals based on a Lennard-Jones intermolecular potential. Substituting (A-1) and (A-7) into (A-6) results in the

following expression for the viscosity of the multicomponent mixture.

$$\mu_{mix} = \frac{\rho \bar{D}}{\mu_1} \sum_{i=1}^{I} \left[\frac{\frac{x_i \mathcal{M}_i}{F_i \mathcal{M}}}{1.385 + \frac{x_i F_i}{\mu_1} \left(\frac{\overset{*}{\Omega}_{ii}}{5} - 1.385 \right)} \right] \qquad \text{(A-8)}$$

and this is the expression utilized to calculate the mixture viscosity output by the ACE program.

Mixture Thermal Conductivity - The thermal conductivity in a polyatomic gas mixture may be represented by (Reference 20)

$$k_{mix} = k_{mono\text{-}mix} + k_{int} \qquad \text{(A-9)}$$

where $k_{mono\text{-}mix}$ is the thermal conductivity in a mixture computed neglecting all internal degrees of freedom and k_{int} is the contribution to the thermal conductivity of the mixture due to the internal degrees of freedom of the molecules. A simplified expression for the mono-mixture thermal conductivity can be derived in a manner similar to the procedure previously discussed for the mixture viscosity. This simplified expression is (from Reference 19)

$$k_{mono\text{-}mix} = \sum_{i=1}^{I} \left[\frac{x_i k_{i\ mono}}{x_i + 1.475 \frac{RT\mu_i}{P\mathcal{M}_i} \sum_{\substack{j=1 \\ j \neq i}}^{I} \frac{x_j}{\mathcal{D}_{ij}}} \right] \qquad \text{(A-10)}$$

where $k_{i\ mono}$ is the thermal conductivity of the pure species i neglecting all internal degrees of freedom of the molecule. The $k_{i\ mono}$ may be expressed in terms of the μ_i as per

$$k_{i\ mono} = \frac{15}{4} \frac{R}{\mathcal{M}_i} \mu_i \qquad \text{(A-11)}$$

The contribution to the thermal conductivity from the internal degrees of

freedom may be expressed as (from Reference 19)

$$k_{int} = \sum_{i=1}^{I} \frac{\rho x_i \frac{\mathcal{M}_i}{\mathcal{M}} \left(C_{pi} - \frac{5}{2} \frac{R}{\mathcal{M}_i} \right)}{\sum_{j=1}^{I} \frac{x_j}{\mathcal{D}_{ij}}} \tag{A-12}$$

By combining (A-1) with (A-9) through (A-12), the mixture thermal conductivity may be written as

$$k_{mix} = \frac{\rho \bar{D}}{\mu_1} \left\{ \sum_{i=1}^{I} \left[\frac{\frac{15}{4} \frac{x_i}{F_i} \frac{R}{\mathcal{M}}}{1.475 + \frac{x_i F_i}{\mu_1} \left(\frac{6A^*_{ii}}{5} - 1.475 \right)} \right] + \frac{\mu_2}{\mathcal{M}} \left[\tilde{C}_p - \frac{5}{2} R\mu_2 \right] \right\} \tag{A-13}$$

where μ_1 and μ_2 are given by (A-4) and (A-5) respectively, and

$$\mu_3 = \sum_{i=1}^{I} \frac{z_i}{\mathcal{M}_i} = \frac{1}{\mu_2} \sum_{i=1}^{I} \frac{x_i}{F_i} \tag{A-14}$$

$$\tilde{C}_p = \sum_{i=1}^{I} z_i C_{pi} \tag{A-15}$$

Thus, (A-13) is the expression utilized to calculate the mixture thermal conductivity output by the ACE program.

Also calculated and output by the ACE program are the Prandtl and Schmidt numbers which are defined here as

$$Pr = \frac{\mu}{k} C_{p\text{-frozen}} \tag{A-16}$$

$$Sc = \frac{\mu_1}{\mu_2} \frac{\mathcal{M}\mu}{\rho \bar{D}} \tag{A-17}$$

The transport properties calculated by the ACE program are all based on the bifurcation approximation for the binary diffusion coefficients expressed in (A-1). This is so even for closed system calculations (in which case diffusion phenomena need not be considered to calculate the chemical and thermodynamic state of the system) and for open system calculations for

which equal diffusion coefficients are assumed (Section 5.3.2). From the equations presented, it may be observed that the properties calculated are highly dependent on the diffusion factors, F_i. Three alternate methods for prescribing the F_i were discussed in Section 5.3.3. The use of the diffusion factor correlation (63) with resident values of $\mathcal{M}_{ref}$ and ε (which were derived primarily from consideration of species diffusion coefficients) should result in reasonably accurate values of other transport properties. Alternately, the correlation (63) may be used with values of $\mathcal{M}_{ref}$ and ε derived by correlating available transport property data for the particular system of interest. If transport properties of maximum accuracy are to be calculated, then the diffusion factors should be input individually for each species. These data may be obtained from tabulations such as Reference 21.

REFERENCES

1. Bartlett, E. P., Rindal, R. A. and Kendall, R. M.: A Critical Evaulation of Recent Developments and Future Requirements for the Prediction of Ablation of Manned Reentry Vehicles at Superorbital Velocities. Vidya Division, Itek Corporation, Palo Alto, California, Vidya Report No. 174, February 4, 1965.

2. Aerotherm Corporation, Mountain View, California, Input Guide, Computer Program for Material Ablation with Chemically Active Boundary Layers in Reentry (MACABRE), September, 1969.

3. Moyer, C. B.: Axi-Symmetric Transient Heating and Material Ablation Program (ASTHMA), Description and User's Manual, Aerotherm Corporation, Mountain View, California, Report No. 68-27, January 15, 1968.

4. Kendall, R. M.: An Analysis of the Coupled Chemically Reacting Boundary Layer and Charring Ablator. Part V; A General Approach to the Thermochemical Solution of Mixed Equilibrium-Nonequilibrium, Homogeneous or Heterogeneous Systems. NASA CR-1064, June 1968 (also published as Aerotherm Report No. 66-7, Part V, March 14, 1967).

5. Powars, C. A., and Kendall, R. M.: User's Manual, Aerotherm Chemical Equilibrium (ACE) Computer Program, Aerotherm Corporation, Mountain View, California, May, 1969.

6. Kendall, R. M., Bartlett, E. P., Rindal, R. A. and Moyer, C. B.: An Analysis of the Coupled Chemically Reacting Boundary Layer and Charring Ablator: Summary Report, NASA CR 1060, June, 1968 (also published as Aerotherm Report No. 66-7, Part I, March 14, 1967.

7. Spalding, D. B.: Convective Mass Transfer, McGraw-Hill Publishing Co., New York, 1963.

8. Moyer, C. B. and Rindal, R. A.: An Analysis of the Coupled Chemically Reacting Boundary Layer and Charring Ablator. Part II; Finite Difference Solution of the In-Depth Response of Charring Materials Considering Surface Chemical and Energy Balances. NASA CR-1061, June 1968 (also published as Aerotherm Report No. 66-7, Part II, March 14, 1967).

9. Bartlett, E. P., and Grose, R. D.: An Evaluation of a Transfer Coefficient Approach for Unequal Diffusion Coefficients, Aerotherm Corporation, Mountain View, California, Report 69-50, June 30, 1969.

10. Kendall, R. M., Rindal, R. A., and Bartlett, E. P.: A Multicomponent Boundary Layer Chemically Coupled to an Ablating Surface. AIAA Journal, Vol. 5, No. 6, June 1967, pp. 1063-1071.

11. Rindal, R. A., Clark, K. J., Moyer, C. B., and Flood, D. T.: Experimental and Theoretical Analysis of Ablative Material Response in a Liquid-Propellant Rocket Engine, Aerotherm Corporation, Palo Alto, California, NASA CR-72301, September 1, 1967.

12. Browne, H. N., Williams, M. N., and Cruise, D. R.: The Theoretical Computation of Equilibrium Compositions, Thermodynamic Properties, and Performance Characteristics of Propellant Systems. U.S. Naval Ordnance Test Station, China Lake, California, NOTS TP 2434, NAVWEPS Report 7043, (ASTIA AD 246591), June 1960.

13. Love, E. S., Woods, W. C., Rainey, R. W., and Ashby, G. C., Jr.: Some Topics in Hypersonic Body Shaping, (AIAA 7th Aerospace Sciences Meeting, New York, January 20-22, 1969) AIAA Paper No. 69-181.

14. Boison, J. C., and Curtiss, H. A.: An Experimental Investigation of Blunt Body Stagnation Point Velocity Gradient, ARS Journal, Vol. 29, No. 2, February 1959, pp 130-135.

15. South, J. C.: Calculation of Axisymmetric Supersonic Flow Past Blunt Bodies with Sonic Corners, Including a Program Description and Listing. NASA TN D-4563, May 1968.

16. Belotserkovskiy, O. M., ed.: Supersonic Gas Flow Around Blunt Bodies. NASA TT F-453, June 1967.

17. McCuen, P. A., Schaefer, J. W., Lundberg, R. E., and Kendall, R. M.: A Study of Solid-Propellant Rocket Motor Exposed Material Behavior. Vidya Division, Itek Corporation, Final Report No. 149, February 1965.

18. Bartlett, E. P. and Kendall, R. M.: Nonsimilar Solution of the Multicomponent Laminar Boundary Layer by an Integral Matrix Method. Aerotherm Corporation Final Report No. 66-7, Part III, March 1967 (also NASA CR 1062, June 1968).

19. Bartlett, E. P., Kendall, R. M., and Rindal, R. A.: An Analysis of the Coupled Chemically Reacting Boundary Layer and Charring Ablator. Part IV; A Unified Approximation for Mixture Transport Properties for Multicomponent Boundary Layer Applications. NASA CR-1063, June 1968 (also published as Aerotherm Report No. 66-7, Part IV, March 14, 1967).

20. Hirschfelder, J. O., Curtiss, C. P., and Bird, R. B.: Molecular Theory of Gases and Liquids. John Wiley and Sons, 1954.

21. Svehla, R. A.: Estimated Viscosities and Thermal Conductivities of Gases at High Temperatures. NASA TR R-132, 1962.

NASA-Langley, 1970 —— 33 CR-1630